

This is the accepted manuscript made available via CHORUS. The article has been published as:

## Low-energy test of second-class current in $\beta$ decays of spin-aligned $^{20}\text{F}$ and $^{20}\text{Na}$

K. Minamisono, T. Nagatomo, K. Matsuta, C. D. P. Levy, Y. Tagishi, M. Ogura, M. Yamaguchi, H. Ota, J. A. Behr, K. P. Jackson, A. Ozawa, M. Fukuda, T. Sumikama, H. Fujiwara, T. Iwakoshi, R. Matsumiya, M. Mihara, A. Chiba, Y. Hashizume, T. Yasuno, and T. Minamisono

Phys. Rev. C **84**, 055501 — Published 16 November 2011

DOI: [10.1103/PhysRevC.84.055501](https://doi.org/10.1103/PhysRevC.84.055501)

# Low Energy Test of SCC in $\beta$ decays of Spin Aligned $^{20}\text{F}$ and $^{20}\text{Na}$

K. Minamisono,<sup>1,2</sup> T. Nagatomo,<sup>3,\*</sup> K. Matsuta,<sup>3</sup> C. D. P. Levy,<sup>4</sup> Y. Tagishi,<sup>5</sup>  
M. Ogura,<sup>3</sup> M. Yamaguchi,<sup>5</sup> H. Ota,<sup>5</sup> J. A. Behr,<sup>4</sup> K. P. Jackson,<sup>4</sup> A. Ozawa,<sup>5</sup>  
M. Fukuda,<sup>3</sup> T. Sumikama,<sup>3,†</sup> H. Fujiwara,<sup>3</sup> T. Iwakoshi,<sup>3</sup> R. Matsumiya,<sup>3</sup>  
M. Mihara,<sup>3</sup> A. Chiba,<sup>5</sup> Y. Hashizume,<sup>5</sup> T. Yasuno,<sup>5</sup> and T. Minamisono<sup>3,‡</sup>

<sup>1</sup>*TRIUMF, 4004 Wesbrook Mall, Vancouver, B. C., Canada, V6T 2A3*

<sup>2</sup>*National Superconducting Cyclotron Laboratory,*

*Michigan State University, East Lansing, MI 48824, USA*

<sup>3</sup>*Department of Physics, Osaka University, Toyonaka 560-0043, Osaka, Japan*

<sup>4</sup>*TRIUMF, 4004 Wesbrook Mall, Vancouver, B. C., V6T 2A3, Canada*

<sup>5</sup>*Department of Physics, University of Tsukuba, Tsukuba 305-8571, Ibaraki, Japan*

## Abstract

The  $G$ -parity violating, second-class current (SCC) induced tensor term in the weak-nucleon axial-vector current was determined from  $\beta$ -decay correlation measurements of the mass  $A = 20$  mirror pair. The alignment correlation terms in the  $\beta$ -decay angular distribution from the purely spin aligned mirror pair,  $^{20}\text{F}$  and  $^{20}\text{Na}$ , were measured for the first time in the present study. Combining the present results with existing results of  $\beta$  and delayed  $\gamma$ -ray angular correlation measurements for the  $A = 20$  mirror pair, the SCC induced tensor term was extracted to be  $d_{\text{II}}/Ac = 0.18 \pm 0.48$ . In the extraction, the weak magnetism term,  $b/Ac = 8.58 \pm 0.28$ , evaluated from the  $M1$  analogue  $\gamma$ -ray decay strength, was used in a framework of the Conserved Vector Current hypothesis. This is the first unambiguous extraction of the  $(b - d_{\text{II}})/Ac$  term free from the contribution of the second-forbidden form factor,  $j_2$ , in the axial-vector current, which was a limiting factor for accurate determination of non-existence of the SSC in the  $\beta$  decay of the  $A = 20$  system.

PACS numbers: 24.80.+y, 27.30.+t, 23.20.En, 23.40.-s

---

\*Present address: Department of Chemistry, International Christian University, Mitaka 181-8585, Tokyo, Japan

†Present address: Department of Physics, Tokyo University of Science, Noda, Chiba 278-8510, Japan

‡Present address: Department for the Application of Nuclear Technology, Fukui University of Technology,

---

Gakuen, Fukui 910-8505, Japan

## I. INTRODUCTION

As a consequence of the unification of weak and electromagnetic interactions in the standard electroweak gauge model [1], the conserved vector current (CVC) hypothesis and absence of the second class current (SCC) [2] are imposed on the weak nucleon currents in a quark model. Many low energy studies have been performed to test the standard electroweak model in nuclear  $\beta$  decay, for which review papers can be found in [3–6]. Weak nuclear processes are described by the current-current-type V-A interaction as  $H_I = \sqrt{1/2}(V_\mu + A_\mu)\{\bar{\psi}_e\gamma_\mu(1 + \gamma_5)\psi_\nu\} + \text{h.c.}$ , where  $V_\mu$  and  $A_\mu$  are the vector and the axial vector currents, respectively. The most general forms of the currents, made up of the Dirac matrices  $\gamma_\mu$  and the four-momentum transfer  $q_\mu$ , are given [7] by

$$\begin{aligned} V_\mu &= \bar{u}(p_2) \left( g_V \gamma_\mu - i \frac{g_M - g_V}{2M} \sigma_{\mu\nu} q^\nu + \frac{g_S}{2M} q_\mu \right) u(p_1), \\ A_\mu &= -\bar{u}(p_2) \gamma_5 \left( g_A \gamma_\mu - i \frac{g_T}{2M} \sigma_{\mu\nu} q^\nu + \frac{g_P}{2M} q_\mu \right) u(p_1). \end{aligned} \quad (1)$$

Here,  $\sigma_{\mu\nu} = [\gamma_\mu, \gamma_\nu]/2i$ ,  $p$  is the four momentum of the parent nucleus and  $M$  is the nucleon mass. Along with the main vector  $g_V$  and the main axial vector  $g_A$  coupling constants for vector and axial-vector currents, respectively, four terms may be induced. They are the weak magnetism  $g_M$ , the induced scalar  $g_S$ , the induced tensor  $g_T$ , and the induced pseudoscalar  $g_P$  currents. In the usual sign convention, those currents, which are transformed as  $GV_\mu G^{-1} = +V_\mu$  for vector current and  $GA_\mu G^{-1} = -A_\mu$  for axial-vector current, are classified as  $G$ -parity regular first-class currents and those transformed opposite are  $G$ -parity irregular second-class currents [2]. Here  $G$  is the transformation defined by the product of the charge conjugation  $C$  and the charge symmetry operation as  $G = C \exp(i\pi T_y)$ , where  $U = \exp(i\pi T_y)$  is the rotation about the  $y$  axis by  $180^\circ$  in the charge space, . If each of the weak-nucleon current,  $V_\mu$  and  $A_\mu$ , has a definite  $G$  parity, the  $g_S$  and  $g_T$  terms should vanish, because they have different  $G$  parities from those of their leading terms.

The presently best tested consequences of CVC are the requirements that the main vector coupling constant should be constant regardless of the nucleus considered, and absence of the SCC induced scalar term. Very careful analysis [8] of  $ft$  values of the 13 best known  $0^+ \rightarrow 0^+$  super allowed transitions confirmed the universality of  $g_V$  at a precision level of  $1.3 \times 10^{-4}$ , and the absence of the induced scalar term,  $m_e f_S / g_V = -(110 \pm 130) \times 10^{-5}$ , where  $m_e$  is the electron rest mass and  $g_S = -2M f_S$ . Another possible SCC in the weak

nucleon current is the induced tensor term in the axial-vector current, where there is no electromagnetic analogue and the axial-vector current is not a conserved current as the CVC is for the vector current. The induced tensor term is currently best constrained to  $2Mf_T/f_A = -0.15 \pm 0.12 \pm 0.05$  at a 90% confidence level by the measurements of  $\beta$ -decay angular distribution from nuclear-spin aligned  $^{12}\text{B}$  and  $^{12}\text{N}$  [9]. Here, form factors are related as  $g_T = -2Mf_T$  and  $g_A = -f_A$ .

Although the induced tensor term is small and there is no indication of SCC, the SCC may be masked by local cancellations [5, 10] possible due to uncertainties in the nuclear structure. Therefore, the search for violation should be undertaken in various mass systems. For this purpose,  $\beta$ -decay correlation measurements were performed in the  $A = 8$  ( $\beta$ - $\alpha$  angular correlation) [11, 12] and in the  $A = 20$  ( $\beta$ - $\gamma$  angular correlation) [13–17] mirror systems. The  $\beta$  decay correlation terms were formulated to first order of recoil terms in [7] and expressions taken in the reference will be used hereafter in this paper. Unambiguous extraction of SCC, however, has been rather difficult from those correlation measurements due to imperfect knowledge of the  $M1/E2$  mixing ratio of  $M1$  analogue  $\gamma$  decays and poor statistical error of the  $\gamma$ -ray decay strengths, from which a second-forbidden form factor,  $f$ , in the vector current is evaluated under an assumption of CVC.

An alternative procedure to extract the SCC induced tensor term was recently introduced in the  $A = 8$  system [18], where the alignment correlation terms in the  $\beta$ -decay angular distribution from nuclear-spin aligned  $^8\text{Li}$  and  $^8\text{B}$  were combined with the  $\beta$ - $\alpha$  angular correlation terms. The  $(b - d_{\text{II}})/Ac$  term and other coupling constants associated with higher-order matrices are independently determined by fitting both correlation terms simultaneously. Here  $b/Ac$  is the weak magnetism,  $d_{\text{II}}/Ac$  is the SCC induced tensor term with  $c$  being Gamow-Teller form factor and  $g_T/g_A = d_{\text{II}}/Ac$ . This procedure combining both correlation terms is a more reliable way to extract the  $(b - d_{\text{II}})/Ac$  term than that with a single correlation measurement. It is noted that the SCC induced tensor term always appears with the weak magnetism in those correlation type measurements, and therefore, precise extraction of the SCC induced tensor term is only possible when the weak magnetism is well known.

The alignment correlation terms of the  $A = 20$  system,  $^{20}\text{F}(I^\pi = 2^+, T_{1/2} = 11.07 \text{ s})$  and  $^{20}\text{Na}(I^\pi = 2^+, T_{1/2} = 447.9 \text{ ms})$ , were measured for the first time in the present study. The result was combined with the existing data on  $\beta$ - $\gamma$  angular correlation measurements for an unambiguous extraction of the  $(b - d_{\text{II}})/Ac$  term. This procedure is particularly important

in the  $A = 20$  system, where a second-forbidden form factor,  $j_2$ , in the axial-vector current contributes to the correlation terms in addition to  $f$ , due to the large difference in  $\beta$ -decay  $Q$  values between  $^{20}\text{F}$  and  $^{20}\text{Na}$ . The  $j_2$  can only be evaluated using theoretical calculations, and therefore, it has been a limiting factor in an accurate determination of the SCC induced tensor term in the  $A = 20$  system [17]. The present result places twice more stringent limit on the SCC induced tensor term in the  $A = 20$  system than the previous one, though the present precision is dominated by the limited statistical errors of the existing data on  $\beta$ - $\gamma$  angular correlation measurements.

## II. $\beta$ -DECAY CORRELATION TERMS

The  $\beta$ -decay angular distribution from a spin-oriented nucleus is given [7] by

$$W(E, \theta) \propto B_0(E) \left\{ 1 + \frac{p}{E} \frac{B_1(E)}{B_0(E)} \mathcal{P} P_1(\cos \theta) + \frac{p^2}{E^2} \frac{B_2(E)}{B_0(E)} \mathcal{A} P_2(\cos \theta) \right\}, \quad (2)$$

where  $E$  and  $p$  are the  $\beta$ -ray total energy and momentum, respectively,  $\theta$  is an angle between the orientation axis and the direction of  $\beta$ -ray momentum,  $P_n(\cos \theta)$  is the Legendre polynomial of rank  $n$ , and  $\mathcal{P}$  and  $\mathcal{A}$  are the polarization and alignment, respectively. The orientations are defined for nuclear spin  $I = 2$  as

$$\begin{aligned} \mathcal{P} &\equiv \frac{\sum m a_m}{I} = \frac{1}{2} (2a_2 + a_1 - a_{-1} - 2a_{-2}), \\ \mathcal{A} &\equiv -1 + 3 \frac{\sum m^2 a_m}{I(I+1)} = a_2 - \frac{1}{2} a_1 - a_0 - \frac{1}{2} a_{-1} + a_{-2}, \end{aligned} \quad (3)$$

where  $a_m$  is the population in the magnetic substate with quantum number  $m$  and is normalized to one,  $\sum a_m = 1$ . For  $\beta$  decays of ground states  $^{20}\text{F}(I^\pi = 2^+, T = 1)$  and  $^{20}\text{Na}(I^\pi = 2^+, T = 1)$  to the first excited 1.634 MeV state in  $^{20}\text{Ne}(I^\pi = 2^+, T = 0)$ , the alignment correlation term,  $B_2/B_0$ , is given by

$$\frac{B_2(E)}{B_0(E)} = -\frac{2}{3} \frac{H_2(E, 0)}{H_0(E)}, \quad (4)$$

where the rank 2 orientation correlation term is given [7] by

$$\begin{aligned} \frac{H_2(E, s)}{H_0(E)} &= \frac{E}{2AM} \left\{ 1 \pm \frac{b - d_{\text{II}}}{c} - \frac{d_{\text{I}}}{c} + (-1)^s \frac{1}{\sqrt{14}} \left( \pm \frac{3f}{c} \pm \sqrt{\frac{3}{2}} \frac{g}{c} \frac{E_0}{AM} + \frac{3j_2}{c} \frac{E_0}{2AM} \right) \right\} \\ &+ \frac{E^2}{2(AM)^2} \left\{ (-1)^s \frac{1}{\sqrt{14}} \left( \mp \sqrt{\frac{3}{2}} \frac{g}{c} - \frac{3j_2}{c} \right) - \frac{3}{\sqrt{35}} \frac{j_3}{c} \right\}, \end{aligned} \quad (5)$$

where  $E$  and  $E_0$  are the  $\beta$ -ray and end point energy, respectively,  $s$  is 0 or 1 and determines the sign of higher order matrices and the upper and lower signs refer to electron and positron decay, respectively. The form factors are weak magnetism  $b$ , Gamow-Teller  $c$ , first class induced tensor  $d_I$ , second class induced tensor  $d_{II}$ , second-forbidden vectors  $f$  and  $g$ , and second-forbidden axial-vectors  $j_2$  and  $j_3$ .

On the other hand, the  $\beta$ - $\gamma$  angular correlation is given [7] by

$$W(E, \theta_{\beta-\gamma}) \propto 1 + a(E) \frac{p}{E} \cos \theta_{\beta-\gamma} + p(E) \frac{p^2}{E^2} \cos^2 \theta_{\beta-\gamma}, \quad (6)$$

where  $\theta_{\beta-\gamma}$  is the angle between momenta of  $\beta$  and subsequent  $\gamma$  rays. For  $\beta$  decays of ground states of  $^{20}\text{F}$  and  $^{20}\text{Na}$  to the first excited state in  $^{20}\text{Ne}$  and subsequent  $\gamma$  decay to the ground state of  $^{20}\text{Ne}(I = 0^+, T = 0)$ , the  $\beta$ - $\gamma$  angular correlation term,  $p(E)$ , is given by

$$p(E) = \frac{1}{2} \frac{H_2(E, 1)}{H_0(E)}. \quad (7)$$

Note that the second-forbidden form factors,  $f$ ,  $g$  and  $j_2$  change their signs from those in the alignment correlation terms, Eq. (4) and (7), due to the sign change of  $s$ . The  $(b - d_{II})/Ac$  term can be isolated from other form factors associated with higher-order matrices and may be extracted as a linear coefficient of  $\beta$ -ray total energy as

$$\left[ \frac{B_2(E)}{B_0(E)} \right]_{\text{F}} - \left[ \frac{B_2(E)}{B_0(E)} \right]_{\text{Na}} - \frac{4}{3} ([p(E)]_{\text{F}} - [p(E)]_{\text{Na}}) = -\frac{b - d_{II}}{Ac} \frac{4}{3M} E. \quad (8)$$

### III. EXPERIMENT

Experiments on  $^{20}\text{F}$  and  $^{20}\text{Na}$  were performed at the Tandem Accelerator Complex of the University of Tsukuba (UTTAC) and at the ISAC facility at TRIUMF, respectively. The alignment correlation terms were extracted from the difference between energy spectra measured with positive and negative alignments, which were produced by converting nuclear polarization into alignment using the  $\beta$ -NMR technique. Highly polarized  $^{20}\text{F}$  and  $^{20}\text{Na}$  were required for efficient and accurate measurements. Details are described in the following sections.

## A. Production and implantation

### 1. $^{20}\text{F}$

Nuclear spin polarized  $^{20}\text{F}$  beam was produced using a polarization transfer reaction,  $^{19}\text{F}(\vec{^2\text{H}},\text{p})\vec{^{20}\text{F}}$ , with a polarized deuteron ( $^2\text{H}$ ) beam provided by the polarized ion source (PIS) combined with a 12 UD pelletron accelerator (12 MV) at UTTAC. A polarized  $^2\text{H}$  beam was produced using the Lamb-shift-type polarizer and a typical degree of polarization was 75% measured by the quench-ratio method [19]. The polarized  $^2\text{H}^-$  ions were injected into the 12 UD pelletron accelerator and accelerated to 6 MeV. Typical intensity of the polarized  $^2\text{H}$  beam was 1.2 nA at a Faraday cup just before the experimental setup. The direction of  $^2\text{H}$  beam polarization was tuned using the Wien filter to be vertical at the experimental port. The polarized  $^2\text{H}$  beam was pulsed using a mechanical beam chopper, which produced a beam on-off ratio of 1. Typically the beam-on (off) time was 16.5 s (16.5 s). The rotation of the chopper was monitored using a photo coupler and used for triggers of the data acquisition.

A schematic view of the experimental setup is shown in Fig. 1. A production target, consisting of a  $\text{MgF}_2$  single crystal ( $100 \pm 10 \mu\text{m}$  in thickness), placed at the center of an NMR magnet also served as an implantation medium for the recoiling  $^{20}\text{F}$ . The  $\text{MgF}_2$  target was tilted by  $45^\circ$  relative to the beam axis, and hence to the direction of an external magnetic field, to stop the incident  $^2\text{H}$  beam in the  $\text{MgF}_2$ , in which the stopping range was about  $100 \mu\text{m}$ . The reaction  $Q$  value to produce  $^{20}\text{F}$  is  $+7.217 \text{ MeV}$ , and the maximum stopping range of  $^{20}\text{F}$  in the  $\text{MgF}_2$  is a few  $\mu\text{m}$ . Therefore, the stopped  $^{20}\text{F}$  nuclei were distributed along the stopping range of the  $^2\text{H}$  beam. The  $\text{MgF}_2$  was surrounded by an rf coil for NMR. An external magnetic field of  $0.2500 \text{ T}$  was applied parallel to the direction of the  $^2\text{H}$  polarization, and the rf field for NMR was applied perpendicular to the external field. The typical  $\beta$ -ray counting rate was  $10^3$  counts per second.

$\beta$ -emitting  $^{25}\text{Al}(T_{1/2} = 7.18 \text{ s})$  and  $^{27}\text{Mg}(T_{1/2} = 9.458 \text{ m})$  were also produced through  $^{24}\text{Mg}(\text{d}, \text{n})^{25}\text{Al}$  and  $^{26}\text{Mg}(\text{d}, \text{p})^{27}\text{Mg}$  reactions, respectively, with Mg isotopes in the  $\text{MgF}_2$  target. The contaminating  $\beta$  rays from  $^{25}\text{Al}$  and  $^{27}\text{Mg}$  reduced the measured polarization of  $^{20}\text{F}$ . This reduction was corrected to obtain the true polarization using a mixing ratio of  $^{25}\text{Al}$  and  $^{27}\text{Mg}$  in the  $^{20}\text{F}$  spectrum. The ratio was determined from the fit of a theoretical

function to the measured energy spectra, which is discussed in section IV C 6. A possible polarization of  $^{25}\text{Al}$ , which may be produced in the nuclear reaction with polarized D beam and maintained in the  $\text{MgF}_2$  target, did not affect the  $\beta$ -NMR measurement of  $^{20}\text{F}$ . This is because the NMR frequencies of  $^{20}\text{F}$  were well separated from those of  $^{25}\text{Al}$  due to the large difference in  $g$ -factors of  $^{20}\text{F}$  and  $^{25}\text{Al}$ .  $^{27}\text{Mg}$  was unpolarized in the  $\text{MgF}_2$  target, due to the long lifetime compared with its polarization relaxation time of the order of 10 s.

## 2. $^{20}\text{Na}$

The 500 MeV proton beam from the TRIUMF cyclotron was used to bombard a SiC production target, which was coupled to a surface ion source. Singly-charged  $^{20}\text{Na}$  ions were extracted at an energy of 40.8 keV and mass separated. The pure  $^{20}\text{Na}$  beam was transported to the polarizer beam line [20] in the ISAC-I experimental hall. The ion beam was first passed through a Na-vapor cell and partially neutralized by charge exchange. After neutralization, Na atoms were polarized using collinear optical pumping on the 589.8 nm (vacuum)  $D_1$  transition ( $3s\ 2S_{1/2} \leftrightarrow 3p\ 2P_{1/2}$ ) with circularly polarized light [21]. The  $\text{Na}^+$  ions, which cannot be polarized, were removed by an electrostatic deflector. The velocity of the  $^{20}\text{Na}$  beam was adjusted to tune the Doppler-shifted laser frequency into resonance with the  $D_1$  transition, by applying a bias voltage to the Na-vapor cell. Both of the ground state hyperfine levels ( $3s\ 2S_{1/2}\ F = I + 1/2$  and  $I - 1/2$ ) were pumped to achieve high polarization using side band frequencies produced by an electro-optic modulator (EOM), a technique that has been successfully employed in the past [22]. The collinear laser light was generated by a frequency-stabilized ring-dye-laser (Coherent 899-21) pumped by a 7-W argon-ion laser. After passing through a 1.9 m interaction region with the laser light, the polarized  $^{20}\text{Na}$  beam was re-ionized in a differentially-pumped He-gas target.

The sign (direction) of  $^{20}\text{Na}$  polarization could be switched by alternating the helicity of the circularly polarized laser light. The magnitude of polarization and its relaxation time in an implantation crystal could be extracted by measuring the asymmetric  $\beta$ -ray angular distribution both from positively and negatively polarized  $^{20}\text{Na}$ . Several implantation media were tested [23] to select a suitable implantation medium for the alignment correlation term measurement. ZnO and Mg single crystals with hexagonal crystalline structure maintained the polarization of Na isotopes with a long relaxation time. Their non-cubic crystalline

structure also provided the well defined electric field gradients required to convert the nuclear polarization into nuclear alignment. Both crystals were used for alignment correlation term measurements.

A pulsed  $^{20}\text{Na}$  beam was used and the implantation time was 500 ms. The 40.8 keV  $^{20}\text{Na}$  beam was stopped on a single crystal surface. The thicknesses of the crystals were  $100 \pm 10 \mu\text{m}$  and  $200 \pm 50 \mu\text{m}$  for ZnO and Mg, respectively. A schematic view of the experimental setup is shown in Fig. 2. The single crystal was placed at the center of an NMR permanent magnet [23] with a central magnetic field of 0.528 T. The single crystal was surrounded by an rf coil. The direction of the external magnetic field was parallel to the direction of  $^{20}\text{Na}$  polarization and the rf field for NMR was applied perpendicular to the external field. The implantation depth into the ZnO single crystal was  $\sim 50 \text{ nm}$ . A V-shaped arrangement of single crystals was used as illustrated in the right side of Fig. 3. Two crystals (each  $10 \text{ mm} \times 7 \text{ mm} \times \sim 200 \mu\text{m}$  thick) were used with the 10 mm sides aligned to give a  $90^\circ$  angle between the crystal faces. Since the implantation depth was very shallow compared to the crystal thickness,  $\beta$  rays measured by detectors placed  $0^\circ$  (u) and  $180^\circ$  (d) relative to the magnetic field direction had a similar scattering effect through the crystal. Possible systematic errors due to correction for the scattering are minimal in the u/d ratio to extract polarization. On the other hand in the  $45^\circ$  arrangement of the crystal (left side of Fig. 3), the correction due to the scattering is very different and may cause a large systematic error in the u/d ratio. The typical  $\beta$ -ray counting rate was  $20 \times 10^3$  counts per second.

## B. Electromagnetic Interaction

The Hamiltonian of the electromagnetic interaction between nuclear moments and external fields [24] is given by

$$H = -\boldsymbol{\mu} \cdot \mathbf{H}_0 + \frac{eqQ}{4I(2I-1)} \{3I_z^2 - I(I+1) + \frac{\eta}{2}(I_+^2 + I_-^2)\}, \quad (9)$$

where  $\boldsymbol{\mu}$  is the magnetic moment,  $\mathbf{H}_0$  is the external magnetic field,  $I_z$  is the third component of the spin operator, and  $I_\pm$  are the spin raising and lowering operators. The largest component of the electric field gradient is defined by  $q = V_{ZZ}$  where  $V$  is the electrostatic potential and  $V_{ii} = d^2V/di^2$  with  $V_{XX} + V_{YY} + V_{ZZ} = 0$ . The asymmetry parameter of the electric field gradient is defined as  $\eta = (V_{XX} - V_{YY})/V_{ZZ}$ , with  $|V_{XX}| \leq |V_{YY}| \leq |V_{ZZ}|$ . An

electric field gradient is provided by the internal field of a single crystal. The energy levels are given by

$$E_m = -g\mu_N H_0 m + \frac{h\nu_Q}{12}(3\cos^2\theta - 1 + \eta\sin^2\theta\cos 2\phi)\{3m^2 - I(I+1)\}, \quad (10)$$

where, for simplicity, the electric-quadrupole interaction is regarded as a perturbation to the main magnetic-dipole interaction. Eq. (10) is given to first-order of the electric-quadrupole coupling constant,  $eqQ/h$ , with  $\nu_Q = 3eqQ/\{2I(2I-1)h\}$  being a normalized electric-quadrupole coupling frequency. In Eq. (10),  $m$  is the magnetic quantum number, and  $\theta$  and  $\phi$  are the Euler angles between the principal axes of the electric field gradient and  $H_0$ . The first term in Eq. (10) gives the  $2I+1$  magnetic substates separated by a fixed energy value, determined from the applied  $H_0$  and the nuclear  $g$  factor, due to the magnetic-dipole interaction (Zeeman splitting). These substates are further shifted by the electric-quadrupole interaction and the energy spacing between adjacent substates is no longer constant. The  $2I$  separate transition frequencies appear as

$$\nu_{m-1\leftrightarrow m} = \nu_L - \frac{\nu_Q}{4}(3\cos^2\theta - 1 + \eta\sin^2\theta\cos 2\phi)(2m-1), \quad (11)$$

since the transition frequencies correspond to the energy difference between two adjacent energy levels ( $\Delta m = \pm 1$ ) in Eq. (10). Here  $\nu_L = g\mu_N H_0/h$  is the Larmor frequency. The variation in the number and position of resonance frequencies between the pure magnetic-dipole interaction and both the magnetic-dipole and electric-quadrupole interactions are schematically shown in Fig. 4 for the case of  $I = 2$ . It is noted that when the electric-quadrupole interaction cannot be considered as a perturbation to the magnetic-dipole interaction, higher-order terms of the electric-quadrupole interaction have to be considered. Higher-order terms were considered for both  $^{20}\text{F}$  in  $\text{MgF}_2$  and  $^{20}\text{Na}$  in  $\text{ZnO}$ , due to the condition of  $|\nu_L| \sim |\nu_Q|$ . For  $^{20}\text{Na}$  in  $\text{Mg}$ , the perturbation technique may be applied because the condition of  $|\nu_L| \gg |\nu_Q|$  is fulfilled for the relevant  $eqQ/h$ .

### C. Quadrupole coupling constant

The quadrupole coupling frequency,  $\nu_Q$ , needed to be known for precise determination of transition frequencies, which were required for the spin manipulation in order to convert nuclear spin polarization into spin alignment. The  $\nu_Q$  was determined in the experiment as a prerequisite for the alignment term measurements.

### 1. $^{20}\text{F}$ in $\text{MgF}_2$

The implanted  $^{20}\text{F}$  occupies a  $^{19}\text{F}$  substitutional site in a  $\text{MgF}_2$  target. The  $\text{MgF}_2$  has a rutile crystalline structure (tetragonal) and the  $c$ -axis was set parallel to the external magnetic field. Conditions of implantation are summarized in Table I. The values of  $eqQ/h$  and  $\eta$  of  $^{20}\text{F}$  in  $\text{MgF}_2$  are known [25] from a  $\beta$ -NMR measurement to be  $eqQ/h = -5.77 \pm 0.02$  MHz and  $\eta = 0.317 \pm 0.002$ . The  $eqQ/h$  value was confirmed in the present study using a multi-frequency NMR technique [26] and determined to be  $|eqQ/h| = 5.7 \pm 0.1$  MHz, which is consistent with the previous one [25].

### 2. $^{20}\text{Na}$ in $\text{ZnO}$ and $\text{Mg}$

The polarized  $^{20}\text{Na}$  beam was implanted into a Mg single crystal, which has a hexagonal close packed crystalline structure. The  $c$ -axis was set parallel to the external magnetic field. Conditions of implantation are summarized in Table I. The  $eqQ/h$  of  $^{20}\text{Na}$  in Mg was determined in the present study using the multi-frequency NMR technique [26] and extracted to be  $|eqQ/h(^{20}\text{Na in Mg})| = 36.7 \pm 0.5$  kHz. The polarized  $^{20}\text{Na}$  beam was also implanted into a ZnO single crystal, which has a hexagonal close packed crystalline structure. The  $c$ -axis was set perpendicular to the external magnetic field. The  $eqQ/h$  of  $^{20}\text{Na}$  in ZnO was determined [27], using the multi-frequency NMR technique, to be  $|eqQ/h(^{20}\text{Na in ZnO})| = 690 \pm 12$  kHz. There appear to be two final locations of Na ions in ZnO, where the crystal lattice provides a different electric-field gradient on Na. Since NMR frequencies of the  $^{20}\text{Na}$  nuclei occupying the minor implantation site (20 %) were well separated from those of the major site (80 %), there was no systematic error in the extraction of polarization associated with the minor implantation site.

## D. Spin manipulation technique

Nuclear polarization was converted into a positive or a negative alignment using an NMR technique (the spin manipulation technique) in the present measurement. This is essential because almost pure alignments with opposite signs can be produced and the large effective alignment (difference between these alignments) makes the measurement more reliable. An adiabatic fast passage (AFP) and a depolarization (DEP) method were used in the NMR

technique to realize the conversion. The AFP interchanged and the DEP equalized populations in two adjacent magnetic sub-states. For nuclei with  $I = 2$  such as  $^{20}\text{F}$  and  $^{20}\text{Na}$ , a single transition frequency (the Larmor frequency) splits into four resonance frequencies, Eq. (11), under the presence of the electric interaction superimposed on the magnetic interaction. The four frequencies are denoted as  $f_1$ ,  $f_2$ ,  $f_3$ , and  $f_4$ , which correspond to transitions between two adjacent magnetic substates,  $m = +2 \leftrightarrow +1$ ,  $+1 \leftrightarrow 0$ ,  $0 \leftrightarrow -1$ , and  $-1 \leftrightarrow -2$ , respectively. The spin manipulation conditions are summarized in Table I.

### 1. *Timing sequence program*

The spin manipulation was performed in accordance with timing sequence programs controlled by a computer. The timing sequence program used for alignment correlation term measurements is shown in Fig.5. A pulsed D beam was used to produce polarized  $^{20}\text{F}$ . The  $^{20}\text{Na}$  beam was pulsed using an electrostatic deflector. Positive and negative alignments were produced in a one beam-count cycle in counting sections III and VIII, where  $\beta$ -ray energy spectra were measured. A possible systematic error that may be caused by a fluctuation of the primary beam intensity [9] could be eliminated by taking the counting ratio between counting sections III and VIII, which is discussed in section IV A. Two timing sequence programs, named  $A_1$  and  $A_2$  and shown in Fig. 5, were used for the production of positive and negative alignments. A positive alignment was produced first in  $A_1$  in counting section III, and a negative alignment was produced in counting section VIII. The duration of counting section III was shorter than VIII to balance the counting statistics between  $\beta$ -ray energy spectra with positive and negative alignments. In  $A_2$ , on the other hand, a negative alignment was produced first, in order to compensate for the relaxation of alignments.

A geometrical asymmetry, due mainly to a small difference in the solid angles and efficiencies of the up and down detectors, had to be eliminated to determine polarization. Three timing sequence programs, named  $P_0$ ,  $P_1$ , and  $P_2$ , were used to determine the geometrical asymmetry and are shown in Fig. 6. Decays of the initial polarization, an inverted polarization produced using a set of 10 AFPs, and twice inverted polarization produced using two sets of 10 AFPs (the resulting polarization pointing in the same direction as the initial polarization) were measured in the  $P_0$ ,  $P_1$ , and  $P_2$  timing sequence programs, respectively. The  $\beta$ -ray up and down counting ratios in a counting section  $i$  for these timing sequence

programs are given as

$$[R_0]_i = g_i \frac{1 + AP_i}{1 - AP_i}, [R_1]_i = g_i \frac{1 + \alpha AP_i}{1 - \alpha AP_i}, [R_2]_i = g_i \frac{1 + \alpha^2 AP_i}{1 - \alpha^2 AP_i}. \quad (12)$$

Here  $g_i$  is the geometrical factor and  $\alpha$  is the inversion efficiency defined as  $P' = \alpha P_0$  with  $P'$  being an inverted polarization. The  $g_i$ ,  $\alpha$ , and  $AP_i$  can be extracted by solving Eq. (12).

The LED in Fig. 5 and 6 indicates light pulse irradiation sections by a temperature stabilized light-emitting diode (LED) for gain stabilization of the  $\beta$ -ray detector. A larger timing structure was repeated until enough counting statistics were accumulated. The structure consisted of five sets of  $A_1$  and  $A_2$  timing sequence programs, two sets of  $P_0$  and  $P_1$  and one set of  $P_2$ , to balance counting statistics for the alignment terms and polarization.

## 2. rf system

A schematic of the rf system for  $\beta$  NMR is shown in Fig. 7. A computer-controlled rf generating system produced an rf signal, which was sent to a 1000-W main amplifier. The amplified signal was applied to an rf coil, which was part of an LC resonance circuit. The circuit included an impedance matching transformer and a bank of four selectable variable capacitors. In the case of  $^{20}\text{Na}$ , for example, after applying the first frequency for 10 ms, another frequency was generated by the rf generating system and sent to the same LC resonance circuit. A different capacitor, which was tuned to satisfy the LC resonance condition for the second frequency, was selected by the fast-switching relay system. The switching time between rf signals was 3 ms. The system ensured sufficient power (the oscillating magnetic field strength,  $H_1 \sim 1$  mT) for a set of four transition frequencies for  $^{20}\text{Na}$  in ZnO/Mg and  $^{20}\text{F}$  in MgF<sub>2</sub>. The experimental conditions for rf in NMR are summarized in Table II. Detail of the rf system is described elsewhere [26].

## E. $\beta$ -ray energy spectrum

### 1. $\beta$ -ray detection system

The  $\beta$ -ray energy was measured using a large plastic scintillator (counter E; 160 mm in diameter and 120 mm long) in coincidence with two thin plastic scintillators. Two separate counters E and coincidence detectors were used for  $^{20}\text{F}$  and  $^{20}\text{Na}$  experiments, and the layout

of the detector systems are illustrated in Fig. 1 and 2. One of the thin plastic scintillators was placed near the implantation crystal (counter A; 22 (12) mm in diameter and 0.5 mm thick) while the other was placed right before counter E (counter B; 76 (55) mm in diameter and 1 mm thick), defining the solid angle of the detector system for the  $^{20}\text{F}$  ( $^{20}\text{Na}$ ) experiment. A cone-shaped air-core plastic scintillator (counter C) was mounted inside the hole of the NMR magnet pole to veto  $\beta$  rays that scattered from the surface of the magnet. All of the  $\beta$  detectors were placed outside the vacuum chamber, and  $\beta$  rays passed through a thin plastic vacuum window (0.1 mm thick) before reaching the detectors. The two detector telescopes were placed at  $0^\circ(\text{u})$  and  $180^\circ(\text{d})$  relative to the direction of polarization.

The voltage applied to the second dynode of the photomultiplier tube of the counter E was dropped for the  $^{20}\text{F}$  experiment during the implantation period to avoid saturation and possible aftereffects. The gain of the energy-detection system was stabilized using a pulsed blue LED, which was embedded in a constant temperature bath. The pulse length and rate were similar to light from the scintillator of counter E at about 10 ns and,  $5 \times 10^3$  and  $1 \times 10^3$  pulses per second for  $^{20}\text{F}$  and  $^{20}\text{Na}$  experiment, respectively. The LED light pulse irradiated the counter E for 100 ms for  $^{20}\text{F}$  and 30 ms for  $^{20}\text{Na}$  at the end of each timing sequence program so as not to disturb  $\beta$ -ray detection.

Typical  $\beta$ -ray energy spectra are shown in Fig.8.  $\beta$  decays of  $^{25}\text{Al}$  ( $Q_{\text{E.C.}} = 4.277$  MeV) and  $^{27}\text{Mg}$  ( $Q_{\beta}^- = 2.61$  MeV) contaminated the low energy part of the  $^{20}\text{F}$  spectrum.  $^{20}\text{Na}$  decays to the excited states in  $^{20}\text{Ne}$  at 7.421 MeV (16.4%), which was detected in addition to the decay to the first excited state at 1.634 MeV (79.3%). Contributions from those  $\beta$  decays to the alignment correlation terms were corrected in the analysis.

## 2. Response function of the $\beta$ detector

The measured  $\beta$ -ray energy spectrum may be given by

$$N_{\beta+\beta\gamma}(E^m) \propto \iiint dE dE^d d\Omega S(E) R_{\beta+\beta\gamma}(E, E^d, \theta_\beta) G(E^m, E^d, \sigma), \quad (13)$$

which contains pileup effects of the 1.634 MeV delayed  $\gamma$  rays, from the first excited state in  $^{20}\text{Ne}$ , following the  $\beta$  decays of  $^{20}\text{F}$  and  $^{20}\text{Na}$ . The energy spectrum is described as a function of measured energy,  $E^m$ , the  $\beta$ -ray spectral shape,  $S(E) \propto pE(E_0 - E)B_0(E)F(Z, E)\{1 + R(E, E_0)\}$ , with  $p$ ,  $E$  and  $E_0$  being  $\beta$ -ray momentum, energy and end-point energy, re-

spectively, the Fermi function  $F(Z, E)$ , and the radiative correction  $R(E, E_0)$ . The energy deposit,  $E^d$ , is defined as  $E^d = E - \Delta E$ , where  $\Delta E$  is the energy loss of electrons/positrons in the implantation crystal and coincidence counters (counter A and B). The energy loss was evaluated using the Monte-Carlo simulation code EGS4 [28] and  $\Delta E$  values of  $277 \pm 4$  keV,  $306 \pm 7$  keV and  $337 \pm 8$  keV were obtained for  $^{20}\text{F}$  in  $\text{MgF}_2$ ,  $^{20}\text{Na}$  in  $\text{Mg}$  and  $^{20}\text{Na}$  in  $\text{ZnO}$  catchers, respectively. The response function,  $R_{\beta+\beta\gamma}(E, E^d, \theta_\beta)$ , was evaluated using the EGS4 simulation code, where an energy deposit,  $E^d$ , of  $\beta$  particle in counter E was simulated for a given incident  $\beta$ -ray energy,  $E$ , and angle,  $\theta_\beta$ , in a realistic geometry and material of the detector system. The delayed 1.634 MeV  $\gamma$  rays were simultaneously simulated to account for the pileup effect. The response functions were simulated for the initial kinetic energy from 0.1 MeV to 5.6 MeV with a 200 keV step for  $^{20}\text{F}$  and from 0.2 MeV to 11.6 MeV with a 200 keV step for  $^{20}\text{Na}$ . Typical results of the simulation are shown in Fig. 9 for 3 MeV electrons (left) and 5 MeV positrons (right). The response function for electrons was simulated with a  $\text{MgF}_2$  crystal and for positrons with  $\text{Mg}$  or  $\text{ZnO}$ . The spectra are shifted by  $\Delta E$  so that the peaks are aligned to the incident  $\beta$ -ray energies. The contribution of the 1.634 MeV pileup  $\gamma$  rays to  $\Delta E$  was negligible. The resolution of the detection system was taken into account by convoluting the Gaussian,  $G(E^m, E^d, \sigma) = \text{Exp}[-(E^d - E^m)^2/2\sigma^2 E^d]/(\sqrt{2\pi}\sigma\sqrt{E^d})$ , where  $\sigma\sqrt{E^d}$  is the resolution of the detection system. The resolutions were determined from the  $\chi^2$  fitting of Eq. (13) to data. Values of  $\sigma = 0.078 \pm 0.004$  MeV $^{1/2}$  and  $0.114 \pm 0.025$  MeV $^{1/2}$  were obtained for the  $^{20}\text{F}$  and  $^{20}\text{Na}$  detection systems, respectively. Results of the fitting to the data are shown in Fig. 8 in dashed curves. The data are well reproduced by the theoretical curve, Eq. (13), indicating validity of the response function simulated by the EGS4. It is noted that the  $\beta$ - $\beta$  pileup effect was negligible compared to the 1.634 MeV  $\gamma$ -ray pileup effect.

### 3. Energy calibration

The energy calibration of the detector system was performed using  $\beta$ -decay end-point energies of several  $\beta$ -emitting nuclei produced online.  $\beta$ -decay end-point energies of  $^{15}\text{O}$ ,  $^{20}\text{F}$ ,  $^{28}\text{Al}$  and  $^{25}\text{Al}$  were used for the  $^{20}\text{F}$  experiment. End-point energies of  $^{20}\text{Na}$  (two branches),  $^{21}\text{Na}$  and  $^{26}\text{Na}$  were used for the  $^{20}\text{Na}$  experiment. A sum of the spectra measured in the timing sequence programs P<sub>0</sub>, P<sub>1</sub> and P<sub>2</sub>, was used for  $^{20}\text{F}$  to minimize distortion of spectra

due to polarization. Distortion of the spectra due to alignment was negligible, since the initial alignment was small. For the  $^{20}\text{Na}$  calibration un-polarized Na beams, produced by turning off the laser, were used to be free from distortion of the spectra due to large initial polarization and alignment. The end-point channel, which corresponded to the maximum kinetic energy deposited in the counter E, was determined from the least  $\chi^2$  fitting of the theoretical  $\beta$ -decay energy spectrum given in Eq. (13).

## IV. ANALYSIS

### A. Extraction of alignment correlation term

The alignment correlation terms were extracted from the  $\beta$ -ray energy spectra measured at counting sections III and VIII in timing sequence programs A<sub>1</sub> and A<sub>2</sub>, where the dominant nuclear orientation was alignment (see section III D). The alignment correlation terms were extracted from a double ratio  $D(E, \theta)$  of  $\beta$ -ray counts at the total energy  $E$  as

$$\left[ \frac{B_2(E)}{B_0(E)} \right] \simeq \frac{D(E, 0^\circ) + D(E, 180^\circ) - 2}{2\tilde{\mathcal{A}}}, \quad (14)$$

where the double ratio is defined as

$$D(E, \theta) \equiv \frac{W(E, \theta)_{A_1^{\text{III}}}}{W(E, \theta)_{A_2^{\text{III}}}} \frac{W(E, \theta)_{A_2^{\text{VIII}}}}{W(E, \theta)_{A_1^{\text{VIII}}}} \simeq 1 \pm \frac{p}{E} \frac{B_1(E)}{B_0(E)} \delta\mathcal{P} + \frac{p^2}{E^2} \frac{B_2(E)}{B_0(E)} \tilde{\mathcal{A}}, \quad (15)$$

where  $W(E, \theta)_{A_i^k}$  is given in Eq. (2) and represents the number of  $\beta$  rays at energy  $E$  detected in the counting section  $k$  in the timing sequence program  $A_i$ . The upper and lower signs are for  $\theta = 0^\circ$  and  $180^\circ$ , respectively. The small but finite residual polarization difference  $\delta\mathcal{P}$  due to imperfect spin manipulation, and the effective alignment  $\tilde{\mathcal{A}}$  are defined as

$$\delta\mathcal{P} = (\mathcal{P}_1^{\text{III}} - \mathcal{P}_1^{\text{VIII}}) + (\mathcal{P}_2^{\text{VIII}} - \mathcal{P}_2^{\text{III}}) \quad (16)$$

$$\tilde{\mathcal{A}} = (\mathcal{A}_1^{\text{III}} - \mathcal{A}_1^{\text{VIII}}) + (\mathcal{A}_2^{\text{VIII}} - \mathcal{A}_2^{\text{III}}). \quad (17)$$

The evaluation of the effective alignment is discussed in the next section and summarized in Table III. The residual polarization is canceled in the simple average of the double ratio in Eq. (14), because the polarization term has opposite signs between  $\theta = 0^\circ$  and  $180^\circ$ . There is a small rank  $n = 3$  orientation,  $\mathcal{T}$ , which is also canceled in the simple average of double ratios.

## B. Evaluation of effective alignment

The effective alignment  $\tilde{\mathcal{A}}$  was calculated using parameters determined by the spin manipulation discussed above. The parameters used were the initial magnetic substate populations  $a_m$  with  $m$  through -2 to 2, the efficiency of AFP to interchange adjacent populations  $\eta$ , the incompleteness of DEP  $\delta$ , and the relaxation constant of polarization  $\lambda_{\mathcal{P}}$ . The  $\eta$  was defined using substate populations  $a'_m$  and  $a'_{m-1}$  after AFP as

$$a'_m = (1 - \eta)a_m + \eta a_{m-1} \quad (18)$$

$$a'_{m-1} = \eta a_m + (1 - \eta)a_{m-1}, \quad (19)$$

where  $\eta$  was assumed to be independent of the transitions and frequency applied. This is justified because each transition was well saturated with high rf amplitude and wide frequency modulation. The  $\delta$  was similarly defined for each transition frequency as

$$a'_m = \{(1 + \delta_m)a_m + (1 - \delta_m)a_{m-1}\} / 2 \quad (20)$$

$$a'_{m-1} = \{(1 - \delta_m)a_m + (1 + \delta_m)a_{m-1}\} / 2. \quad (21)$$

This is because very subtle control of rf amplitude, frequency modulation, and number of sweeps (typically 5 to 10 times), were required to achieve good equalization between two adjacent populations. The decay constant for orientation of rank  $n$  was set to  $n(n+1)\lambda_{\mathcal{P}}/2$ , assuming purely statistical decay of  $a_m$ . Orientations up to rank  $n = 4$  were taken into account in the fitting procedure. The results of the fit to the spin manipulations are shown in Fig. 10, 11 and 12 for  $^{20}\text{F}$  in  $\text{MgF}_2$ ,  $^{20}\text{Na}$  in  $\text{ZnO}$  and  $^{20}\text{Na}$  in  $\text{Mg}$ , respectively. In the figures, the open and solid circles are for  $A_1$  and  $A_2$  timing sequence programs, respectively and dots are for the  $P_0$  timing sequence program. The vertical bar is statistical error and the horizontal bar indicates counting duration of the section. The dashed lines are the results of the fits, which are summarized in Table III together with the effective orientations calculated from the results of the fit. As seen in the table, positive and negative alignments were produced depending on the initial polarization, the signs of the  $g$  factor and  $eqQ/h$ , and the order of applied rf.

### C. Systematic corrections and uncertainties

Corrections to the alignment correlation terms were applied as

$$\left[ \frac{B_2(E)}{B_0(E)} \right]_{\text{corr.}} = C(E) \times \left( \left[ \frac{B_2(E)}{B_0(E)} \right]_{\text{uncor.}} - D_\gamma(E) \right), \quad (22)$$

where  $C(E) = \prod_i C_i(E)$  is the total correction factor to be applied to the alignment correlation term over  $i$  different corrections. The  $D_\gamma(E)$  is a correction for the anisotropic distribution of the delayed 1.634 MeV  $\gamma$  rays from the first excited state in  $^{20}\text{Ne}$  to be subtracted from the alignment correlation term. The corrections are summarized in Tables IV, V and VI for  $^{20}\text{F}$  in  $\text{MgF}_2$ ,  $^{20}\text{Na}$  in  $\text{ZnO}$  and  $^{20}\text{Na}$  in  $\text{Mg}$ , respectively together with systematic uncertainties associated with those corrections. The systematic uncertainty for a correction was evaluated by estimating errors of possible sources,  $\Delta$ , as

$$\Delta C_i(E) = \left| (C_i(E) - 1) \left[ \frac{B_2(E)}{B_0(E)} \right]_{\text{uncor.}} \right| \sqrt{\sum_j \Delta_j^2}, \quad (23)$$

$$\Delta D_\gamma(E) = |D_\gamma(E)| \sqrt{\sum_j \Delta_j^2}. \quad (24)$$

Here  $j$  is for different sources of the uncertainty.

#### 1. Response of the energy detection system

The measured  $\beta$ -ray energy in counter E contains contributions from  $\beta$  rays with different energies, due to the response of the detector system to the  $\beta$  and the 1.634 MeV delayed  $\gamma$  rays. The center of gravity of each energy bin  $E_i$  with a width of  $2\delta E$  was defined as

$$\langle E_i \rangle = \frac{\int_{E_i-\delta E}^{E_i+\delta E} dE^m \iiint dE d\Omega dE^d S(E) R_{\beta+\beta\gamma}(E, E^d, \theta_\beta) EG(E^m, E^d, \sigma)}{\int_{E_i-\delta E}^{E_i+\delta E} dE^m \iiint dE d\Omega dE^d S(E) R_{\beta+\beta\gamma}(E, E^d, \theta_\beta) G(E^m, E^d, \sigma)}, \quad (25)$$

where  $E^d \equiv E - \Delta E$  with  $\Delta E$  being the energy loss of the  $\beta$  particle due to the implantation stopper and thin coincidence counters, as discussed in section III E. The measured alignment correlation terms may be expressed as a linear function of the total energy,  $E_T$ , up to the second power (Eq. (4) and (5)) with coefficients  $\kappa^{(1)}$  and  $\kappa^{(2)}$  such that

$$\left[ \frac{B_2(E_T)}{B_0(E_T)} \right]_{\text{uncor.}} = \kappa^{(1)} \langle E_T \rangle + \kappa^{(2)} \langle E_T^2 \rangle, \quad (26)$$

where  $E_T \equiv E + m_e$ ,  $\langle E_T \rangle = \langle E \rangle + m_e$  and  $\langle E_T^2 \rangle = \langle E^2 \rangle + 2m_e \langle E \rangle + m_e^2$ . The alignment correlation term can be given with the correction for detector response,  $C_{\text{res}}$ , by

$$\left[ \frac{B_2(E_T)}{B_0(E_T)} \right]_{\text{uncor}} = \{ \kappa^{(1)}(E + m_e) + \kappa^{(2)}(E + m_e)^2 \} \frac{\kappa^{(1)} \langle E_T \rangle + \kappa^{(2)} \langle E_T^2 \rangle}{\kappa^{(1)}(E + m_e) + \kappa^{(2)}(E + m_e)^2} \quad (27)$$

$$\equiv \frac{B_2(E_T)}{B_0(E_T)} \frac{1}{C_{\text{res}}(E_T)}. \quad (28)$$

The correction factor  $C_{\text{res}}$  can be extracted from the ratio  $\kappa^{(2)}/\kappa^{(1)}$ , which was evaluated by an iterative fitting of Eq. (26) to the corrected alignment correlation term, starting with rough values of  $C_{\text{res}}$ . The iteration was repeated until  $C_{\text{res}}$  converged. The  $\kappa^{(2)}/\kappa^{(1)}$  values of  $0.34 \pm 0.15 \text{ MeV}^{-1}$  and  $-0.0368 \pm 0.0036 \text{ MeV}^{-1}$  were obtained for  $^{20}\text{F}$  and  $^{20}\text{Na}$ , respectively, and were used for the final  $C_{\text{res}}$ . The systematic uncertainties of the correction were assumed to result from the evaluations of energy resolution of counter E ( $\Delta = 0.2$ ), the low-energy tail of the response function ( $\Delta = 0.1$ ), the  $\gamma$ -ray detection efficiency ( $\Delta = 0.05$ ) and the effect of the external magnetic field on  $\beta$ -ray trajectories ( $\Delta = 1$ ) in the EGS4 simulations for the response function. The evaluation of  $\kappa^{(2)}/\kappa^{(1)}$  ( $\Delta = 0.5$ ) was also considered.

## 2. Solid angle

The solid angle of the detection system is determined by the geometrical layout of counter E and the coincidence detector counter B. In addition to the geometrical effect, scattering of  $\beta$  particles on the implantation stopper caused energy dependent variation of the solid angle. The measured alignment correlation term may be given with the solid angle correction  $C_\Omega$  by

$$\left[ \frac{B_2(E)}{B_0(E)} \right]_{\text{uncor}} \propto \left[ \mathcal{A} \frac{B_2(E)}{B_0(E)} \right]_{\text{uncor}} \frac{1}{\mathcal{A}_{\text{cal}}} \propto \frac{\langle P_2(\cos \theta) \rangle B_2(E)}{\langle P_1(\cos \theta) \rangle B_0(E)} \equiv \frac{1}{C_\Omega(E)} \frac{B_2(E)}{B_0(E)}, \quad (29)$$

where  $\mathcal{A}_{\text{cal}}$  is a calculated alignment from the measured polarization, which is  $P_1(\cos \theta)$  dependent, whereas  $\mathcal{A}$  depends on  $P_2(\cos \theta)$ . The average,  $\langle \ \rangle$  was evaluated as

$$\langle X \rangle = \frac{\int dE^m \iiint dE d\Omega dE^d S(E) R_{\beta+\beta\gamma}(E, E^d, \theta_\beta) X G(E^m, E^d, \sigma)}{\int dE^m \iiint dE d\Omega dE^d S(E) R_{\beta+\beta\gamma}(E, E^d, \theta_\beta) G(E^m, E^d, \sigma)}. \quad (30)$$

The average  $\langle P_1(\cos \theta) \rangle$  was evaluated by integrating the energy spectrum over the energy range used to calculate polarization,  $E^m > 2.5 \text{ MeV}$  for  $^{20}\text{F}$  and  $E^m > 4.0 \text{ MeV}$  for  $^{20}\text{Na}$ . The

average  $\langle P_2(\cos\theta) \rangle$  was evaluated by integrating the energy spectrum over each energy bin,  $E^m = E_i \pm \delta E$ , since the alignment correlation terms were evaluated at each energy bin. The systematic uncertainties of the correction were assumed to result from evaluations of  $\beta$ -ray scattering on various materials ( $\Delta = 0.1$ ) and the effect of the external magnetic field on  $\beta$ -ray trajectories ( $\Delta = 1$ ) in the EGS4 simulations for the response function. Misalignments of the detection system also caused systematic uncertainties through small changes of the solid angle. They were evaluated to be 0.005 for  $^{20}\text{F}$  and 0.004 for  $^{20}\text{Na}$ , which are independent of  $\beta$ -ray energies and quadratically added to  $\Delta C$ .

### 3. Longitudinal polarization of electron

The polarization and alignment dependent terms contain  $p/E$  and  $(p/E)^2$  terms respectively, due to the longitudinal polarization of emitted electrons in  $\beta$  decay, where  $p$  is the  $\beta$ -particle momentum. The measured alignment correlation term may be given with the correction  $C_{p/E}$  for the  $p/E$  by

$$\left[ \frac{B_2(E)}{B_0(E)} \right]_{\text{uncor}} \propto \frac{\langle (\frac{p}{E})^2 \rangle B_2(E)}{\langle \frac{p}{E} \rangle B_0(E)} \equiv \frac{1}{C_{p/E}(E)} \frac{B_2(E)}{B_0(E)}, \quad (31)$$

where the average  $\langle p/E \rangle$  was taken over the entire energy region analyzed since the term is associated with the polarization. For the average  $\langle (p/E)^2 \rangle$ , the integration was taken over each energy bin since the term is associated with the alignment correlation term. The systematic uncertainties of the correction were assumed to result from evaluations of  $\beta$ -ray scattering on various materials ( $\Delta = 0.1$ ) and the effect of the external magnetic field on  $\beta$ -ray trajectories ( $\Delta = 1$ ) in the EGS4 simulations for the response function.

### 4. Polarization correlation term

The polarization correlation term has a small  $\beta$ -ray energy dependence,  $B_1(E)/B_0(E)$  [7], which affects the measured polarization. The alignment correlation term may be given with correction for the  $B_1/B_0$ ,  $C_{B_1}$ , by

$$\left[ \frac{B_2(E)}{B_0(E)} \right]_{\text{uncor}} \propto \frac{1}{\langle \frac{B_1(E)}{B_0(E)} \rangle} \frac{B_2(E)}{B_0(E)} \equiv \frac{1}{C_{B_1}} \frac{B_2(E)}{B_0(E)}. \quad (32)$$

The average  $\langle B_1(E)/B_0(E) \rangle$  was evaluated over the entire energy region analyzed, since the term is associated with the polarization. The matrices required to evaluate  $B_1(E)/B_0(E)$

were obtained from an iterative fitting of the corrected alignment correlation terms, starting with a rough value for  $C_{B_1}$ . The iteration was repeated until  $C_{B_1}$  converged.  $b/Ac = 8.5 \pm 0.5$ ,  $d_1/Ac = 7.5 \pm 0.1$ ,  $g/A^2c = -65 \pm 35$  and  $j_2/A^2c = -300 \pm 300$  were obtained and used only to evaluate  $C_{B_1}$ . The systematic uncertainties of the correction were evaluated based on the errors on those matrix elements and  $\Delta C_{B_1}/C_{B_1} = 0.031$  and  $0.025$  were obtained for  $^{20}\text{F}$  and  $^{20}\text{Na}$ , respectively.

### 5. $\beta$ -decay branches of $^{20}\text{Na}$

The ground state  $^{20}\text{Na}$  ( $I^\pi = 2^+$ ,  $T = 0$ ) mostly decays to the 1.634 MeV first excited state ( $2^+$ ,  $0$ ) and to the 7.42 MeV state ( $2^+$ ,  $0$ ) in  $^{20}\text{Ne}$  with 79.3 % and 16.4 % branching ratio, respectively. The spectral shape,  $S(E)$ , may be expressed with correction for the branching,  $C_{\text{br}}$ , as

$$S(E) \sim S_1(E) \left( 1 + \frac{B_2(E)}{B_0(E)} \mathcal{A}P_2(\cos \theta) \right) + S_2(E) \left( 1 + \frac{B'_2(E)}{B'_0(E)} \mathcal{A}P_2(\cos \theta) \right) \quad (33)$$

$$= S_{\text{tot}}(E) \left\{ 1 + \frac{S_1(E)}{S_{\text{tot}}} \left( 1 + \frac{S_2(E)B'_2(E)/B'_0(E)}{S_1(E)B_2(E)/B_0(E)} \right) \frac{B_2(E)}{B_0(E)} \mathcal{A}P_2(\cos \theta) \right\} \quad (34)$$

$$\equiv S_{\text{tot}}(E) \left( 1 + \frac{1}{C_{\text{br}}(E)} \frac{B_2(E)}{B_0(E)} \mathcal{A}P_2(\cos \theta) \right), \quad (35)$$

where  $S_1$  and  $S_2$  are the spectral shape for decays to the 1.634 MeV and 7.42 MeV states respectively.  $S_{\text{tot}}(E) = S_1(E) + S_2(E)$  and  $\int S_{\text{tot}}(E)dE = 1$ . The  $B'$  indicates correlation terms for decay to the 7.42 MeV state, whose matrices are different from those for decay to the 1.634 MeV state. The matrices calculated in [29, 30] were used to evaluate  $B$  and  $B'$  to obtain  $C_{\text{br}}$ . The systematic uncertainties were evaluated based on the variation of matrix elements calculated in those references [29, 30] and  $\Delta = 0.15$  was obtained.

### 6. Contaminants in $^{20}\text{F}$ energy spectra

$^{20}\text{F}$  was produced by bombarding a  $\text{MgF}_2$  target with  $^2\text{H}$  beam. Due to reactions with Mg isotopes in the  $\text{MgF}_2$ ,  $^{25}\text{Al}$  ( $Q_\beta = 3.255$  MeV,  $T_{1/2} = 7.183$  s) and  $^{27}\text{Mg}$  (1.767 MeV, 9.458 m) were also produced. The fraction of  $^{20}\text{F}$  in the measured spectra was proportional to the measured degree of polarization since  $^{25}\text{Al}$  and  $^{27}\text{Mg}$  were not polarized. The energy

spectrum measured in counting section  $i$  may be expressed as

$$N(i, E) = N_0 S(E, E_0) \frac{2e^{-\lambda t_i}}{\lambda} \sinh\left(\frac{\lambda w_i}{2}\right), \quad (36)$$

where  $\lambda$  is the decay constant and  $t_i$  and  $w_i$  are the central time and duration of counting section  $i$ , respectively.  $N_0$  is a normalization factor and  $S(E, E_0)$  is the  $\beta$ -decay spectral shape. The total energy spectrum in counting section  $i$  can then be given by

$$N_{\text{tot}}(i, E) = N_{20\text{F}}(i, E) + N_{25\text{Al}}(i, E) + N_{27\text{Mg}}(i, E), \quad (37)$$

which was used to fit the energy spectrum in each counting section to determine the  $^{20}\text{F}$  fraction. The  $\beta$  decays of  $^{20}\text{F}$ ,  $^{25}\text{Al}$  and  $^{27}\text{Mg}$  have different end point energies and the corrections were calculated energy as well as time dependently. The measured polarization can be expressed with correction for the mixing,  $C_{\text{mix}}$ , as

$$[\mathcal{P}_i]_{\text{uncor}} = \mathcal{P}_i \int \frac{N_{20\text{F}}(i, E)}{N_{\text{tot}}(i, E)} dE \equiv \mathcal{P}_i \frac{1}{C_{\text{mix}}(i)}, \quad (38)$$

where  $\mathcal{P}_i$  is polarization in counting section  $i$  and the integration was taken for  $E > 2.8$  MeV, which was the energy region analyzed to extract polarization. The measured  $^{20}\text{F}$  polarization was thus corrected before the fitting was applied to the data on polarization change, to extract the degree of alignment and higher order orientations. The corrections are summarized in Table VII. The corrections for distortions of the energy spectra due to contamination were taken into account through the calculation of the effective alignment, since the correction is dependent on time and energy. The effective alignment defined in Eq. (17) was modified as

$$\tilde{\mathcal{A}} = C_{\text{mix}}(\text{III}, E_k)(\mathcal{A}_1^{\text{III}} - \mathcal{A}_2^{\text{III}}) - C_{\text{mix}}(\text{VIII}, E_k)(\mathcal{A}_1^{\text{VIII}} - \mathcal{A}_2^{\text{VIII}}). \quad (39)$$

Here,  $C_{\text{mix}}$  was evaluated by taking the integration in Eq. (38) over each energy bin,  $E_k \pm \delta E$ , and summarized in Table VIII. Since  $C_{\text{mix}}$  was essentially determined by measured energy spectra,  $1\sigma$  statistical errors were considered as the systematic uncertainties of the correction.

### 7. Anisotropic angular distribution of 1.634 MeV delayed $\gamma$ ray

The  $\beta$  decay from the ground states of  $^{20}\text{F}(2^+, 0)$  and  $^{20}\text{Na}(2^+, 0)$  to the first excited state in  $^{20}\text{Ne}(2^+, 0)$  are followed by a 1.634 MeV  $E2$   $\gamma$  ray to the ground state of  $^{20}\text{Ne}(2^+, 0)$ ,

which was partially detected in counter E as a pileup event and distorted the  $\beta$ -decay energy spectrum. The distortion of the spectrum was taken into account in the correction for the response function of the detection system discussed in sections III E 2 and IV C 1. The  $E2$   $\gamma$  decay has an anisotropic angular distribution due to the even-rank orientations of the parent nuclei, which is propagated to the first excited state in  $^{20}\text{Ne}$ . The anisotropic distribution causes a spurious effect in the alignment correlation term, which has to be corrected. The measured  $\beta$ -decay energy spectrum from an oriented nucleus may be given by

$$N_{\beta}(E^m) \propto \iiint dE dE^d d\Omega R_{\beta}(E, E^d, \theta) S(E) (1 + \beta(E, \theta)) G(E^m, E^d, \sigma), \quad (40)$$

and for the  $\beta\gamma$  pileup spectrum by

$$N_{\beta\gamma}(E^d) \propto \iiint dE dE^d d\Omega R_{\beta\gamma}(E, E^d, \theta) S(E) (1 + \beta(E, \theta) + \mathcal{O}_{\gamma}) G(E^m, E^d, \sigma). \quad (41)$$

Here, the spectral shapes are normalized to unity,  $\int S(E) dE = 1$ . The response functions,  $R_{\beta}$  and  $R_{\beta\gamma}$ , are for  $\beta$  rays and  $\beta$ - $\gamma$  pileup events, respectively and  $R_{\beta\gamma}$  is given by

$$R_{\beta\gamma}(E, E^d, \theta) = \int dE_{\gamma}^d R_{\gamma}(E_{\gamma}^d) R_{\beta}(E, E^d, \theta), \quad (42)$$

with  $R_{\gamma}$  being the response function of the 1.634 MeV  $\gamma$  rays, which was evaluated using the EGS4 simulation code. The angle and orientation dependent parts can be expressed [31, 32] as

$$\beta(E, \theta) \simeq \frac{B_2(E)}{B_0(E)} \mathcal{A} P_2(\cos \theta), \quad (43)$$

$$\mathcal{O}_{\gamma} \simeq -\frac{5}{14} \mathcal{A} \langle P_2(\cos \theta_{\gamma}) \rangle_{\Omega_{\gamma}} + \frac{8}{7} \mathcal{Q} \langle P_4(\cos \theta_{\gamma}) \rangle_{\Omega_{\gamma}}, \quad (44)$$

where higher order terms such as the polarization correlation term and terms related to odd-rank orientations are neglected.  $\mathcal{Q}$  is the parent-nucleus orientation of rank 4 and  $\langle P_i \rangle_{\Omega_{\gamma}}$  is the Legendre polynomial of rank  $i$  averaged over the  $\gamma$ -ray detection solid angle. By defining a ratio as

$$r \equiv \frac{\epsilon_{\gamma} \int N_{\beta\gamma}(E^m) dE^m}{\int N_{\beta}(E^m) dE^m}, \quad (45)$$

the measured energy spectrum can be expressed as

$$\begin{aligned} N_{\beta+\beta\gamma}(E^m) &= (1 - r) N_{\beta}(E^m) + r N_{\beta\gamma}(E^m) \\ &\propto \iiint dE dE^d d\Omega \left\{ R_{\beta+\beta\gamma}(E, E^d, \theta) S(E) (1 + \beta(E, \theta)) \right. \\ &\quad \left. + (R_{\beta+\beta\gamma}(E, E^d, \theta) - R_{\beta}(E, E^d, \theta)) S(E) \mathcal{O}_{\gamma} \right\} G(E^m, E^d, \sigma) \\ &\equiv S_{\beta+\beta\gamma}(E^m) \left( 1 + [\beta(E, \theta)]_{\text{uncor.}} + \frac{S_{\beta+\beta\gamma}(E^m) - S_{\beta}(E^m)}{S_{\beta+\beta\gamma}(E^m)} \mathcal{O}_{\gamma} \right), \end{aligned} \quad (46)$$

where  $S_{\beta+\beta\gamma}$  is the energy spectrum from a non-oriented nucleus and  $R_{\beta+\beta\gamma}$  is the total response function defined by

$$R_{\beta+\beta\gamma}(E, E^d, \theta) \equiv (1 - \epsilon_\gamma)R_\beta(E, E^d, \theta) + \epsilon_\gamma R_{\beta\gamma}(E, E^d, \theta). \quad (47)$$

Here,  $\epsilon_\gamma$  is the  $\gamma$ -ray detection efficiency integrated over the  $\gamma$ -ray detection solid angle, which was evaluated using the EGS4 simulation code to be 0.0318 and 0.0265 for  $^{20}\text{F}$  and  $^{20}\text{Na}$  detection systems, respectively. The  $[\beta(E, \theta)]_{\text{uncor.}}$  is the measured and uncorrected alignment correlation term. Now the simple sum of the double ratio given in Eq. (14) is modified as

$$\frac{D(E^m, 0^\circ) + D(E^m, 180^\circ) - 2}{2\tilde{\mathcal{A}}} \simeq \left[ \frac{B_2(E)}{B_0(E)} \right]_{\text{uncor.}} + \frac{S_{\beta+\beta\gamma}(E^m) - S_\beta(E^m)}{S_{\beta+\beta\gamma}(E^m)} \tilde{\mathcal{O}}, \quad (48)$$

with

$$\tilde{\mathcal{O}} = -\frac{5}{14} \langle P_2(\cos \theta_\gamma) \rangle_{\Omega_\gamma} + \frac{8}{7} \frac{\tilde{\mathcal{Q}}}{\tilde{\mathcal{A}}} \langle P_4(\cos \theta_\gamma) \rangle_{\Omega_\gamma}, \quad (49)$$

$$\tilde{\mathcal{Q}} = (\mathcal{Q}_1^{\text{III}} - \mathcal{Q}_1^{\text{VIII}}) + (\mathcal{Q}_2^{\text{VIII}} - \mathcal{Q}_2^{\text{III}}). \quad (50)$$

The correction for the anisotropic angular distribution of the pileup 1.634 MeV  $\gamma$  ray is then given by

$$D_\gamma(E^m) \equiv \frac{S_{\beta+\beta\gamma}(E^m) - S_\beta(E^m)}{S_{\beta+\beta\gamma}(E^m)} \tilde{\mathcal{O}}. \quad (51)$$

The systematic uncertainties of the correction were assumed to result from the evaluation of  $\tilde{\mathcal{O}}$ , for which the  $1\sigma$  statistical error was taken, the misalignment of the detection system ( $\Delta = 0.05$  and  $0.03$  for  $^{20}\text{F}$  and  $^{20}\text{Na}$ , respectively) and the mis-identification of  $\beta$ - $\beta$  coincident events as  $\beta$ - $\gamma$  coincident events ( $\Delta = 0.05$ ). The evaluations of  $\gamma$ -ray detection efficiency ( $\Delta = 0.05$ ), the effect of the external magnetic field on  $\beta$ -ray trajectories ( $\Delta = 1$ ) and the energy resolution of counter E ( $\Delta = 0.2$ ) in the EGS4 simulations for the response function were also considered.

#### D. Corrected alignment correlation term

The corrected alignment correlation terms are shown in Fig. 13 and summarized in Table IX for  $^{20}\text{F}$  and in Table X for  $^{20}\text{Na}$ . The systematic error for each data point is a quadratic sum of all the systematic errors associated with the corrections, and the systematic error caused by the calculation of  $\tilde{\mathcal{A}}$ , for which  $1\sigma$  statistical errors were used since  $\tilde{\mathcal{A}}$  is

a measured quantity. The weighted average of alignment correlation terms of  $^{20}\text{Na}$  in Mg and  $^{20}\text{Na}$  in ZnO were taken as the final result. The statistical errors were used for weights of the mean. The systematic errors are simple average of separately evaluated systematic errors of alignment correlation terms for  $^{20}\text{Na}$  in Mg and  $^{20}\text{Na}$  in ZnO. Taking the weighted mean of the  $^{20}\text{Na}$  data is justified because the corrected alignment correlation terms of  $^{20}\text{Na}$  in Mg and  $^{20}\text{Na}$  in ZnO are consistent within errors.

### E. $\beta$ - $\gamma$ angular correlation experiments

There are three complete sets of data of  $\beta$ - $\gamma$  angular correlation measurements performed by Dupuis-Rolin et al. [13, 14], Tribble et al. [15, 16] and Rosa et al. [17]. The results for  $^{20}\text{F}$  are consistent among these data sets. Dupuis-Rolin et. al reported the  $^{20}\text{Na}$  result in [13] and later modified the data to account for the finite geometry of their gas-cell  $\beta$  source [14]. The modified  $^{20}\text{Na}$  result [14], however, disagrees with the other two  $\beta$ - $\gamma$  results. The present alignment correlation terms defined in Eq. (4) and the normalized  $\beta$ - $\gamma$  correlation terms,  $-4/3p(E) = -2H_2(E, 1)/(3H_0(E))$ , are shown in Fig. 13. The normalized  $\beta$ - $\gamma$  angular correlation term only differs from the alignment correlation term in the sign of higher order matrices. The general trend of the alignment and  $\beta$ - $\gamma$  correlation terms are consistent and therefore it is implied that contributions from the higher order matrices,  $f$ ,  $g$  and  $j_2$  are small, although the  $^{20}\text{Na}$   $\beta$ - $\gamma$  data scatter widely. It is noted that the  $^{20}\text{Na}$   $\beta$ - $\gamma$  data of Dupuis-Rolin et al. [14] are consistently smaller than the other  $\beta$ - $\gamma$  results.

### F. Weak Magnetism

The weak magnetism term,  $b/Ac$ , can be deduced from the  $M1$  analogue  $\gamma$ -ray decay strength,  $\Gamma_{M1}$ , under the CVC hypothesis as

$$b = \sqrt{\frac{6\Gamma_{M1}M^2}{\alpha E_\gamma^3}} = 43.4 \pm 1.2, \quad (52)$$

where  $M$  is the nuclear mass,  $\alpha = 1/137$  is the fine-structure constant, and  $E_\gamma$  is the transition energy between the 10.275 MeV analogue state ( $I^\pi = 2^+$ ,  $T = 1$ ) and the 1.634 MeV first excited state ( $2^+$ ,  $0$ ) in  $^{20}\text{Ne}$ . A weighted average of four measurements of  $\Gamma_{M1}$

[30, 33–36] was used for the evaluation:

$$\Gamma_{M1} = 4.26 \pm 0.23 \text{ eV}. \quad (53)$$

The Gamow-Teller form factor can be related to  $ft$  values as

$$c^2 = \frac{2ft_0}{ft_{20}}, \quad (54)$$

where  $ft_0$  is the  $ft$  value of Fermi super-allowed  $\beta$  transitions and  $ft_{20}$  is the  $ft$  value of the  $A = 20$   $\beta$  decays. Using  $ft$  values of the 13 most precise results of  $0^+ \rightarrow 0^+$  super allowed transitions [8],  $ft_0 = 3072.08 \pm 0.79$  s was obtained. The  $ft_{20}$  was evaluated from  $\log ft$  values of  $^{20}\text{F}$  and  $^{20}\text{Na}$  decays as

$$\log ft_{20} = \frac{\log ft_{20}(^{20}\text{F}) + \log ft_{20}(^{20}\text{Na})}{2} = 4.983 \pm 0.007 \text{ s}, \quad (55)$$

using  $\log ft_{20}(^{20}\text{F}) = 4.9753 \pm 0.0007$  s [37–39] and  $\log ft_{20}(^{20}\text{Na}) = 4.990 \pm 0.005$  s [40, 41]. The difference of  $ft$  values of about 3% between  $^{20}\text{F}$  and  $^{20}\text{Na}$  was quoted as an error to the  $\log ft_{20}$ . The  $ft$  values difference implies the magnitude of the isospin symmetry breaking, for which no corrections were made in the present study, because it is negligible compared to the magnitude of the final error on  $d_{\text{II}}/Ac$ . The Gamow-Teller form factor was obtained as

$$c = 0.253 \pm 0.004. \quad (56)$$

The weak magnetism was then evaluated as

$$\frac{b}{Ac} = 8.58 \pm 0.28, \quad (57)$$

which was used to extract the SCC induced tensor term in the present study.

## V. RESULTS AND DISCUSSION

The  $(b - d_{\text{II}})/Ac$  term and other matrices were determined from a simultaneous fit of the theoretical curve, Eq. (5), to alignment and  $\beta$ - $\gamma$  correlation terms. The fitting was applied to each  $\beta$ - $\gamma$  correlation measurement with the present alignment term and the results are summarized in Table XI. The fitting results are shown in Fig. 13 in solid and dashed curves for the present data and for  $\beta$ - $\gamma$  correlation terms, respectively. A simple average of the present data and the  $\beta$ - $\gamma$  correlation term by Tribble et al. [15, 16], and the present data

and the  $\beta$ - $\gamma$  correlation term by Rosa et al. [17] were conservatively taken as a final result. The data in [14] was not used for the extraction of the final results because the data in [14] disagrees with the other two  $\beta$ - $\gamma$  correlation terms and the simultaneous fit of the theoretical curve to the present data and the data in [14] could not reproduce those data well. The  $(b - d_{\text{II}})/Ac$  term was determined to be

$$\frac{b - d_{\text{II}}}{Ac} = 8.41 \pm 0.31 \text{ (stat.)} \pm 0.24 \text{ (syst.)}. \quad (58)$$

The systematic error was evaluated by applying the simultaneous fit to the alignment correlation terms corrected for  $C_i - \Delta C_i$  and  $C_i + \Delta C_i$ , and the difference of the obtained  $(b - d_{\text{II}})/Ac$  term was taken as the systematic error associated with the correction  $C_i$ . The same procedure was applied for evaluation of systematic error caused by  $D_\gamma$  and the calculation of  $\tilde{\mathcal{A}}$ . The total systematic error was a quadratic sum of all systematic errors caused by the  $C$ ,  $D_\gamma$  and calculation of  $\tilde{\mathcal{A}}$ , which are summarized in Table XII. The induced tensor term can be evaluated using the weak magnetism,  $b/Ac = 8.58 \pm 0.28$  obtained from the analogue  $M1$   $\gamma$ -ray decay strength, as

$$\begin{aligned} \frac{d_{\text{II}}}{Ac} &= 0.18 \pm 0.42 \text{ (stat.)} \pm 0.24 \text{ (syst.)} \\ &= 0.18 \pm 0.48 \text{ (total)}, \end{aligned} \quad (59)$$

where the total error is a quadratic sum of the statistical and systematic errors. The present result is consistent with the absence of SCC in the weak-nucleon axial-vector current. The result is compared to the previous value of the weighted average of  $\beta$ - $\gamma$  correlation measurements [17],  $d_{\text{II}}/Ac = -0.4 \pm 1.1$ , where the error contains 100% uncertainty in the evaluation of  $j_2$ . The present value is consistent with, more accurate than, and twice as precise as the previous value. The non-existence of the SCC induced tensor term in the  $A = 20$  system is consistent with other  $\beta$ -decay correlation measurements in the  $A = 8$  system [18],  $d_{\text{II}}/Ac = -0.24 \pm 0.31$ , and the  $A = 12$  system [9],  $d_{\text{II}}/Ac = -0.15 \pm 0.17$ . It is noted that the error of the present result is dominated by the limited statistical errors of the existing  $\beta$ - $\gamma$  angular correlation measurements.  $\beta$ - $\gamma$  correlation measurements with similar error levels to that of the present alignment correlation terms are highly required for a more precise determination of  $(b - d_{\text{II}})/Ac$ .

A theoretical calculation for  $d_{\text{II}}/Ac$  was performed based on the QCD sum rules [42]. In this QCD framework  $d_{\text{II}}/Ac$  is proportional to the mass difference between the up and down

current quarks estimated roughly to be  $(m_u - m_d)/M \sim 0.004$ . The calculation gives  $d_{\text{II}}/Ac = +0.0152 \pm 0.0053$ , which is consistent with the present experimental limit, though the experimental error is large. Here the free quark masses,  $m_u = 5$  MeV and  $m_d = 9$  MeV, were used and it is noted that the contribution of the electromagnetic effect is small. If this calculation is considered as a fundamental limit of the induced tensor term, experiments may search for the SCC in the window between the experimental and theoretical values, by reducing experimental errors.

On the other hand, in  $\beta$  decay of complex nuclei, any  $G$ -parity irregular signal may result from the  $NNe\nu$  vertex and meson exchange current effects. The KDR model [10] takes into account the mesonic contribution and the off the mass-shell effect. The process  $\omega \rightarrow \pi e\nu$  is considered to be the most likely direct mesonic source of a  $G$ -parity violating current, since the  $\omega N\bar{N}$  coupling constant is large and the  $\omega$  is the lightest meson with appropriate quantum numbers. The  $\omega$  meson is emitted by one nucleon and the  $\pi$  is absorbed by another, the  $\omega \rightarrow \pi e\nu$  decay taking place between the two nucleons. This  $\omega \rightarrow \pi e\nu$  process is  $G$ -parity irregular because  $\omega$  and  $\pi$  are of the same  $G$  parity while the  $G$  parity associated with the leading term changes sign in the axial-vector nucleon current. Nucleons are on the off-shell in a complex nucleus and the induced tensor term takes the expanded form [10], which is given, using  $g_T/g_A = d_{\text{II}}/Ac$ , by

$$ig_T\sigma_{\lambda\rho}k_\rho\gamma_5 \rightarrow i(g'_T\sigma_{\lambda\rho}k_\rho\gamma_5 + ig''_TP_\lambda\gamma_5). \quad (60)$$

Here the second term is associated with an exchange- $\pi$  induced  $N\bar{N}$ -pair and  $k$  and  $P$  refer to the difference and the sum of the initial and final nucleon four-momenta, respectively. This leads to defining the constant

$$2M\zeta = g'_T + g''_T. \quad (61)$$

The  $\omega \rightarrow \pi e\nu$  exchange term is measured by a form factor  $F_\omega$ , which leads to the exchange related constant

$$\lambda = \frac{m_\pi^3 g_{\pi NN}^2}{24\pi M^2} \left( \frac{g''_T}{2M} - \frac{g_{\omega NN} F_\omega}{g_{\pi NN} m_\omega^2} \right), \quad (62)$$

where  $g_{\pi NN}$  and  $g_{\omega NN}$  are  $\pi$ -nucleon and  $\omega$ -nucleus coupling constants, respectively. In the KDR model, the  $\beta$ -decay correlation term is expressed as

$$\kappa = \zeta + \lambda L \approx \frac{g_T}{2M}, \quad (63)$$

where  $L$  is the matrix element of the two-body-transition operators [10, 43, 44]. Therefore, the  $G$ -parity irregular observables may be expressed with a combination of  $\zeta$  and  $\lambda$  and these contributions cannot be separated in a single experiment on a single pair of mirror transitions. Using the present result of  $\kappa = (0.12 \pm 0.33) \times 10^{-3} \text{ MeV}^{-1}$ , together with results of  $\beta$ -decay correlation measurements in the  $A = 8$  [18] system,  $\kappa = -(0.16 \pm 0.20) \times 10^{-3} \text{ MeV}^{-1}$ , and in the  $A = 12$  [9] system,  $\kappa = -(0.10 \pm 0.09) \times 10^{-3} \text{ MeV}^{-1}$ , the KDR parameters are constrained at a  $1\sigma$  level as shown in Fig. 14. In the extraction, the values of  $L$  without short range correlation [44] were used. The KDR parameters are constrained inside a set of parallel lines for each correlation measurement, whose slope is determined by  $L$ . It is clear that a single correlation measurement cannot set any constraint on KDR parameters. The solid ellipse is a  $1\sigma$  contour determined by these three sets of correlation measurements. The KDR parameters are constrained to be

$$\begin{aligned}\zeta &= -(0.10 \pm 0.13) \times 10^{-3} \text{ MeV}^{-1}, \\ \lambda &= -(0.10 \pm 0.77) \times 10^{-3}.\end{aligned}\tag{64}$$

The results are consistent with absence of the SCC, though the error on  $\lambda$  is rather poor. Here it has to be noted that the present and the  $A = 8$  [18] results were not corrected for nuclear structure dependent binding energy effects, which was taken into account in the analysis of the  $A = 12$  system [9]. Such studies will be more useful once experimental errors in the  $A = 8$  and 20 systems become comparable to that of the  $A = 12$  result. Also, studies on the two-body-transition operators,  $L$ , are highly needed, using up-to-date nuclear theories.

## VI. CONCLUSION

The alignment correlation terms in the  $\beta$ -decay angular distributions from the purely spin aligned  $A = 20$  mirror pair,  $^{20}\text{F}$  and  $^{20}\text{Na}$ , were measured for the first time to study the  $G$ -parity irregular, SCC induced tensor term in the weak-nucleon axial-vector current. The  $^{20}\text{F}$  experiment was performed at the UTTAC at University of Tsukuba, using polarized deuteron beam to produce highly polarized  $^{20}\text{F}$ . The  $^{20}\text{Na}$  experiment was performed at the ISAC-I facility at TRIUMF, using optically pumped highly polarized  $^{20}\text{Na}$ . The alignment correlation terms and the angular correlation between the  $\beta$  decay and delayed  $\gamma$  decay from

the first excited 1.634 MeV state to the ground state of  $^{20}\text{Ne}$  have similar sensitivity to the SCC induced tensor term, except for contributions from the higher order terms. Combining the present result with  $\beta$ - $\gamma$  angular correlation measurements, the term with weak magnetism and the SCC induced tensor term,  $(b - d_{\text{II}})/Ac$ , were unambiguously extracted. Here the contributions from forbidden matrices,  $f$  in the vector current and  $j_2$  in the axial-vector current, were removed, which was a limiting factor for an accurate determination of the SCC induced tensor term in the  $A = 20$  system, due to the large difference in  $\beta$ -decay  $Q$  values. The present procedure to combine both correlation terms is a more reliable way to extract the  $(b - d_{\text{II}})/Ac$  term than that with a single  $\beta$ -decay correlation measurement. The term was determined to be  $(b - d_{\text{II}})/Ac = 8.41 \pm 0.31(\text{stat.}) \pm 0.24(\text{syst.})$ . Using the weak magnetism,  $b/Ac = 8.58 \pm 0.28$ , evaluated from the  $M1$  analogue  $\gamma$ -ray decay strength, the SCC induced tensor term was extracted as  $d_{\text{II}}/Ac = 0.18 \pm 0.48$ . The present result is consistent with the absence of the SCC in the weak-nucleon axial-vector current. The present result is also consistent with, more accurate than, and twice as precise as the previous result of  $\beta$ - $\gamma$  correlation measurements,  $d_{\text{II}}/Ac = -0.4 \pm 1.1$ , where a 100% systematic uncertainty was considered in the evaluation of  $j_2$ . A  $\beta$ - $\gamma$  angular correlation measurement with less statistical error is highly required for more precise determination of the SCC induced tensor term in the  $A = 20$  system. The meson-exchange and the off-the-mass-shell effects of a nucleon in a nucleus are considered in a framework of the KDR model. The amplitude of the  $G$ -parity irregular KDR parameters,  $\zeta$  and  $\lambda$ , are constrained using the present result together with the results of other  $\beta$ -decay correlation measurements in the  $A = 8$  and 12 mirror systems. The KDR parameters are determined to be  $\zeta = -(0.10 \pm 0.13) \times 10^{-3} \text{ MeV}^{-1}$  and  $\lambda = -(0.10 \pm 0.77) \times 10^{-3}$ . The result is consistent with non-existence of the SSC.

## ACKNOWLEDGMENTS

The authors are grateful to the UTTAC and TRIUMF staffs. The study was supported in part by Grants-in-Aid for Scientific Research from the Japan Society for the Promotion of Science and by the 21st century COE program, Toward a new basic science: Depth and synthesis. One of the authors (K. M. at NSCL/MSU) would like to thank the supports from the National Science Foundation, Grant PHY06-06007.

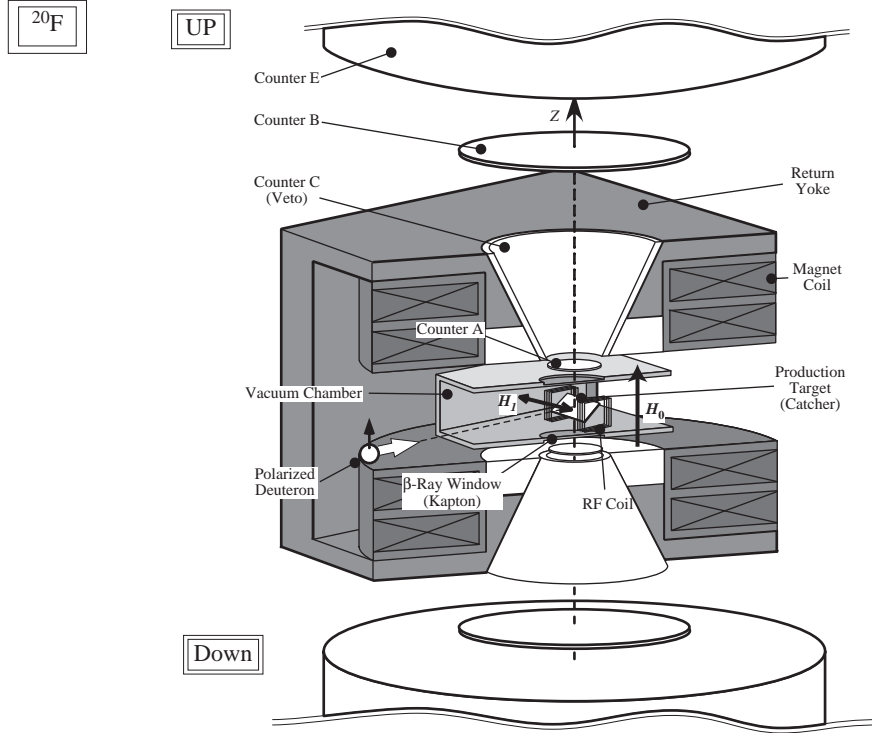


FIG. 1: Schematic of experimental setup for  $^{20}\text{F}$ . A  $\text{MgF}_2$  single crystal was placed at the center of the NMR magnet and an rf coil surrounded the crystal for the rf in the NMR technique. The  $\text{MgF}_2$  was tilted by  $45^\circ$  relative to the beam axis and the direction of  $H_0$ . The rf field was applied perpendicular to the  $H_0$ .  $\beta$  rays were detected using two sets of plastic scintillator telescopes placed at  $0^\circ$  and  $180^\circ$  relative to the polarization direction.

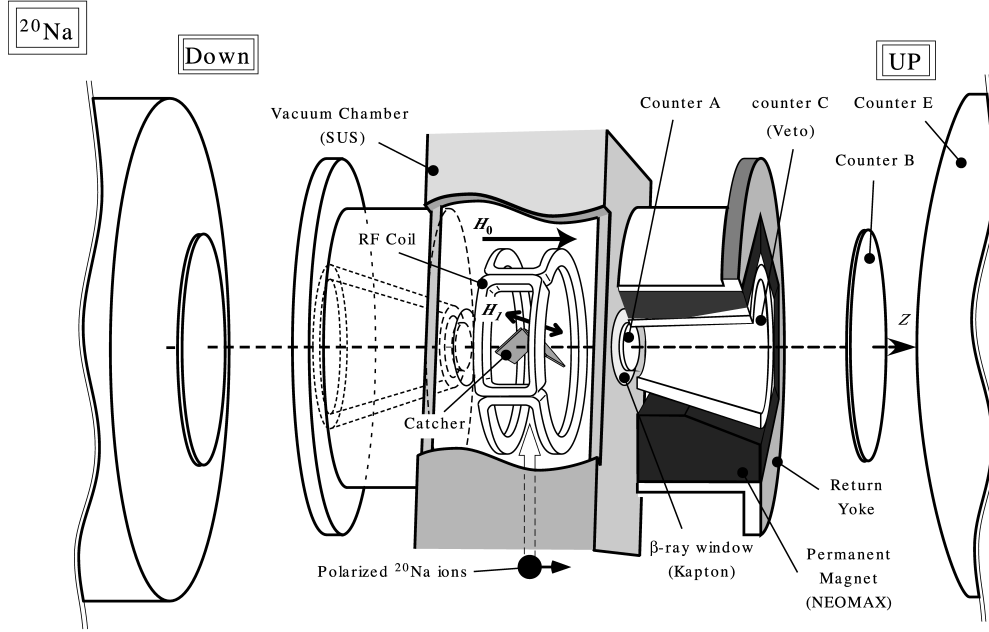


FIG. 2: Schematic of experimental setup for  $^{20}\text{Na}$ . A Mg or a ZnO single crystal was placed at the center of the NMR magnet and an rf coil surrounded the crystal for the rf in the NMR technique. The implantation crystal was arranged to have a V-shaped configuration. The rf field was applied perpendicular to the  $H_0$ .  $\beta$  rays were detected using two sets of plastic scintillator telescopes placed at  $0^\circ$  and  $180^\circ$  relative to the polarization direction.

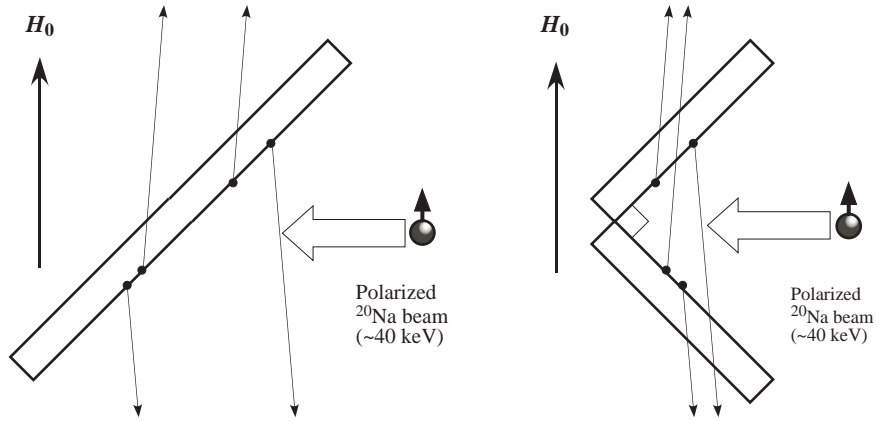


FIG. 3: Arrangement of the implantation crystal. Scattering effect of  $\beta$  particles through the implantation crystal is different between the  $45^\circ$  arrangement (left) and the V-shaped arrangement (right), since the implantation depth is shallow. The V-shaped arrangement was used in the  $^{20}\text{Na}$  experiments.

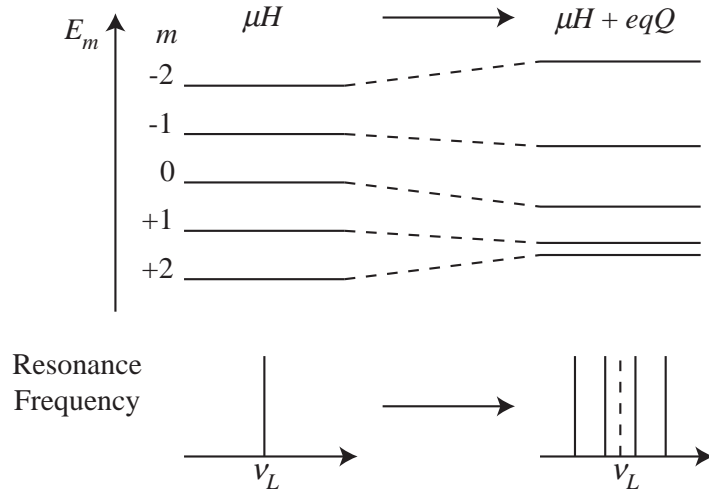


FIG. 4: Energy levels and transition frequencies for an  $I = 2$  nucleus. Energy levels are shown in the presence of a purely magnetic-dipole interaction (left). A single resonance frequency ( $\nu_L$ , the Larmor frequency) results, due to the evenly spaced energy levels. When the electric-quadrupole interaction is added (right), the spacings between adjacent substates become uneven and  $2I$  different resonance frequencies result.

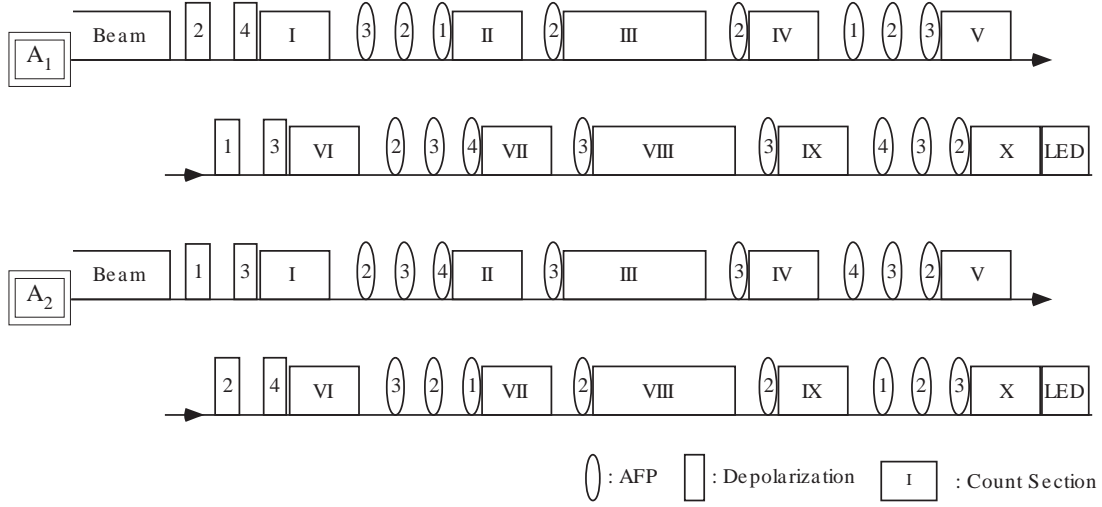


FIG. 5: Timing sequence programs, A<sub>1</sub> and A<sub>2</sub>, for measurements of alignment correlation terms. The roman numerals indicate  $\beta$ -ray counting sections. The arabic numerals indicate rf applied with 1, 2, 3, and 4 corresponding to the  $m = +2 \leftrightarrow +1$ ,  $+1 \leftrightarrow 0$ ,  $0 \leftrightarrow -1$ , and  $-1 \leftrightarrow -2$  transitions, respectively. The LED irradiation time is indicated as LED.

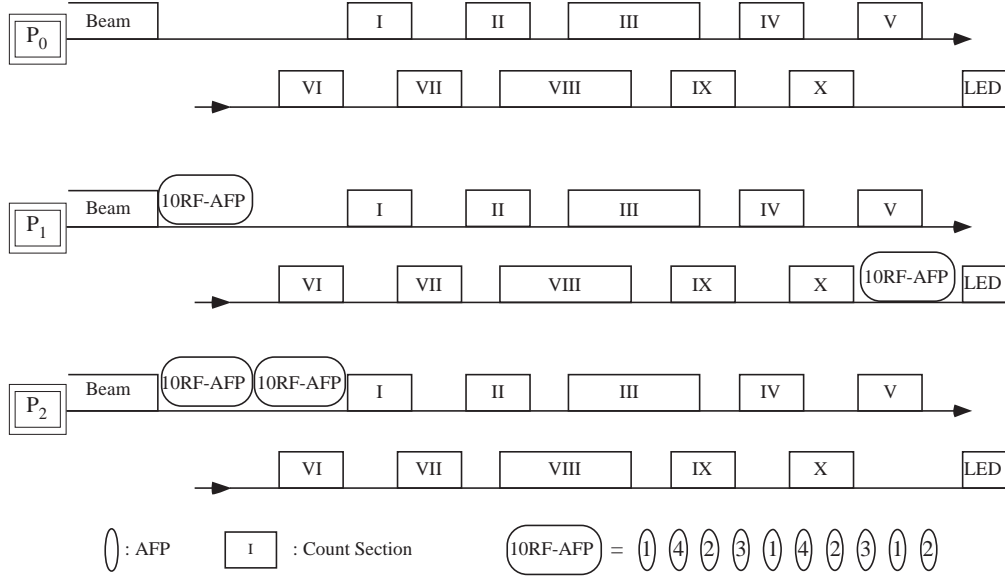


FIG. 6: Timing sequence programs,  $P_0$ ,  $P_1$  and  $P_2$ , for determination of geometrical asymmetry. The roman numerals indicate  $\beta$ -ray counting sections. The arabic numerals indicate rf applied with 1, 2, 3, and 4 corresponding to the  $m = +2 \leftrightarrow +1$ ,  $+1 \leftrightarrow 0$ ,  $0 \leftrightarrow -1$ , and  $-1 \leftrightarrow -2$  transitions, respectively. The LED irradiation time is indicated as LED.

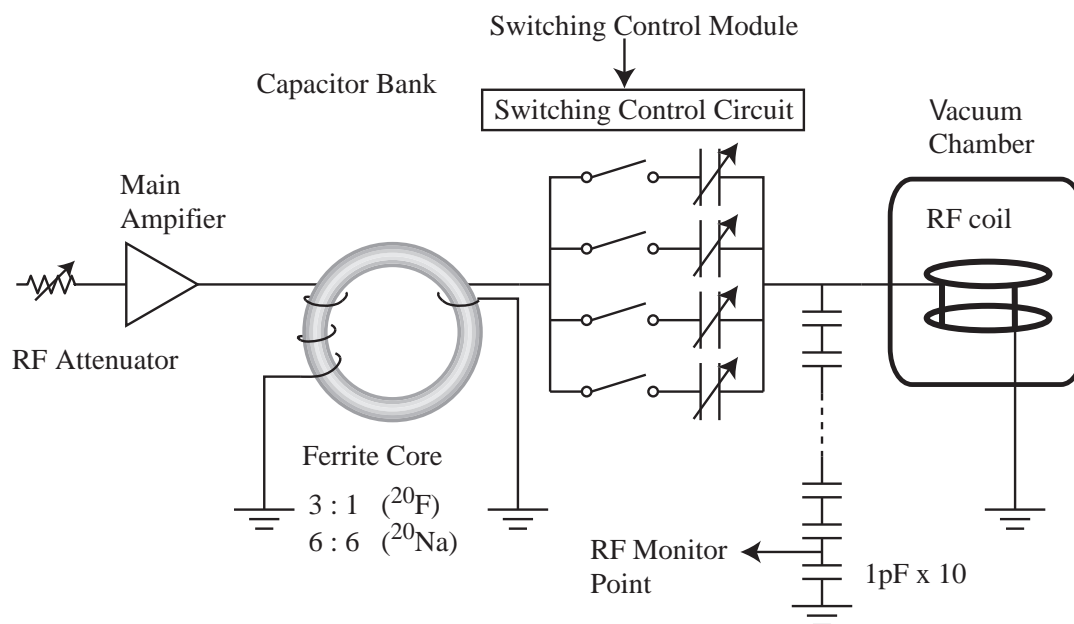


FIG. 7: Rf system for NMR. The rf circuit consists of an rf coil and variable capacitor and makes up an LC resonance circuit. A ferrite core was used for impedance matching. The vacuum capacitors were sequentially selected by fast switching relays in accordance with the timing sequence program.

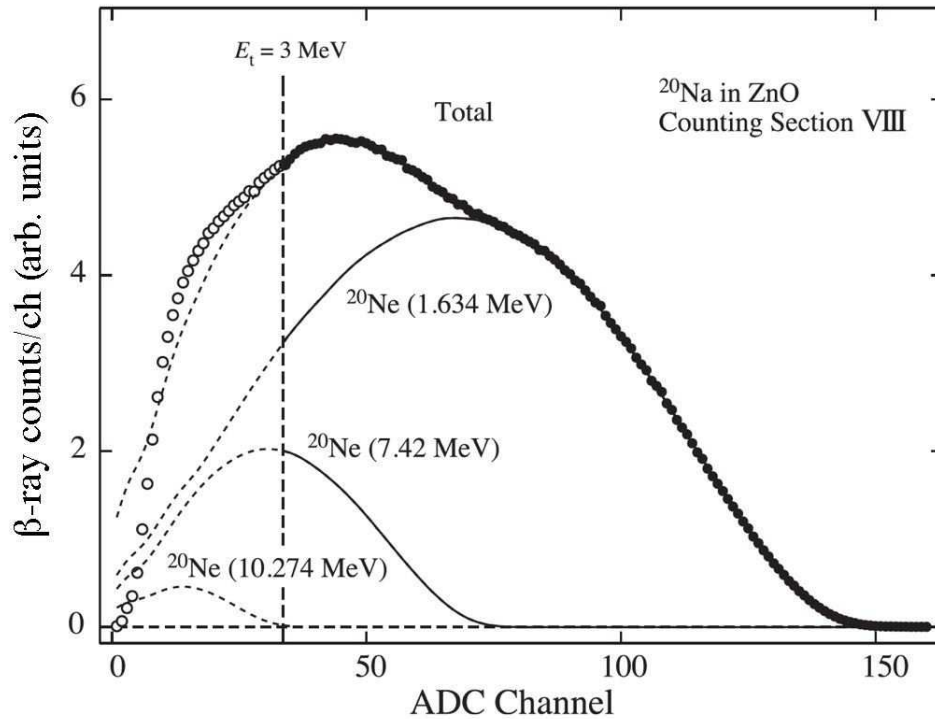
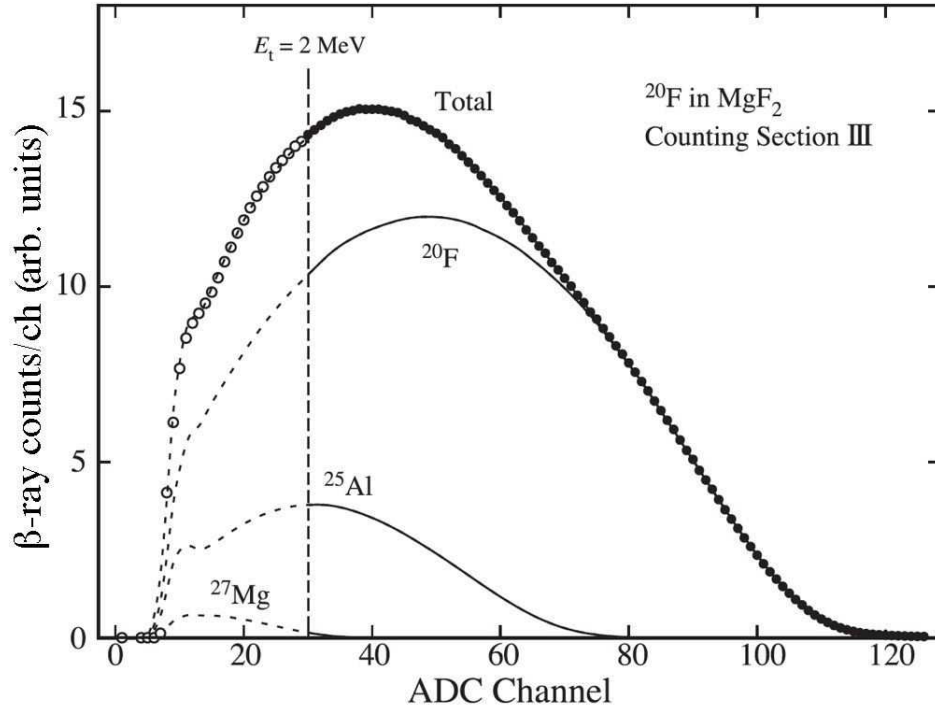


FIG. 8: Typical energy spectra of  $^{20}\text{F}$  (upper) and  $^{20}\text{Na}$  (lower). The  $^{20}\text{F}$  spectrum is contaminated by  $^{25}\text{Al}$  and  $^{27}\text{Mg}$ , produced in the nuclear reaction. The  $^{20}\text{Na}$  spectrum contains the decay to excited states at 7.42 MeV and 10.274 MeV in  $^{20}\text{Ne}$  in addition to the main branch to the first excited state at 1.634 MeV.

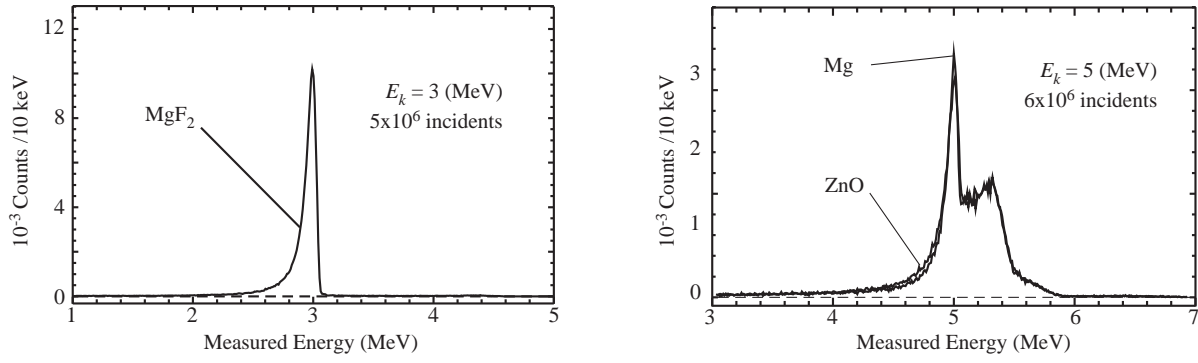


FIG. 9: Response functions of the detector system simulated using EGS4. The results of 3 MeV electrons (left) and 5 MeV positrons (right) are shown. The labels MgF<sub>2</sub>, Mg and ZnO indicate results of simulation with those crystals as implantation media. The spectra are shifted by  $\Delta E$ .

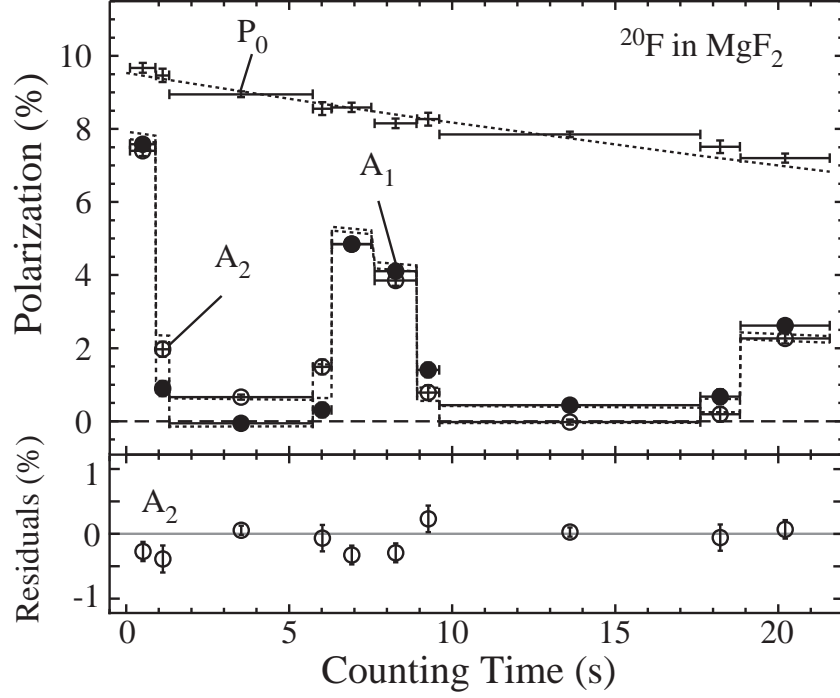


FIG. 10: Results of the spin manipulation for  $^{20}\text{F}$  in  $\text{MgF}_2$ . The change of polarizations are shown as a function of time. The timing sequence programs  $A_1$ ,  $A_2$  and  $P_0$  are shown for  $^{20}\text{F}$  in  $\text{MgF}_2$ . The solid circles are for  $A_1$ , the open circles are for  $A_2$  and the dots are for  $P_0$ . The horizontal bars indicate the counting duration. The dashed lines are the results of the fit and residuals of the fit for  $A_2$  are shown in the lower part of the figure. Rfs were applied between counting sections to manipulate polarization in  $A_1$  and  $A_2$ . In  $P_0$ , the decay of initial polarization was measured with no rf applied.

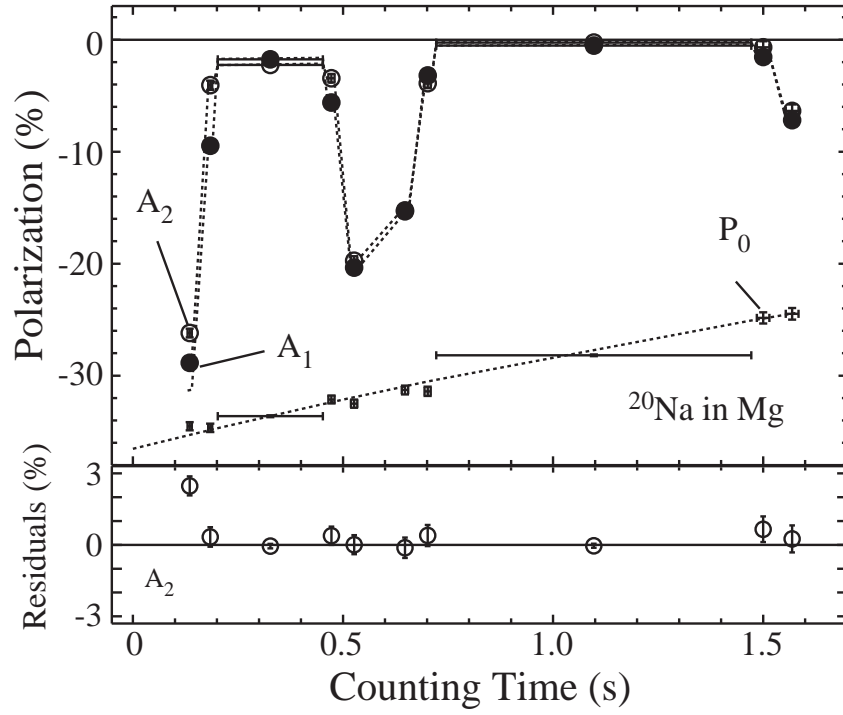


FIG. 11: Results of the spin manipulation for  $^{20}\text{Na}$  in ZnO. See the figure caption for Fig. 10. for details.

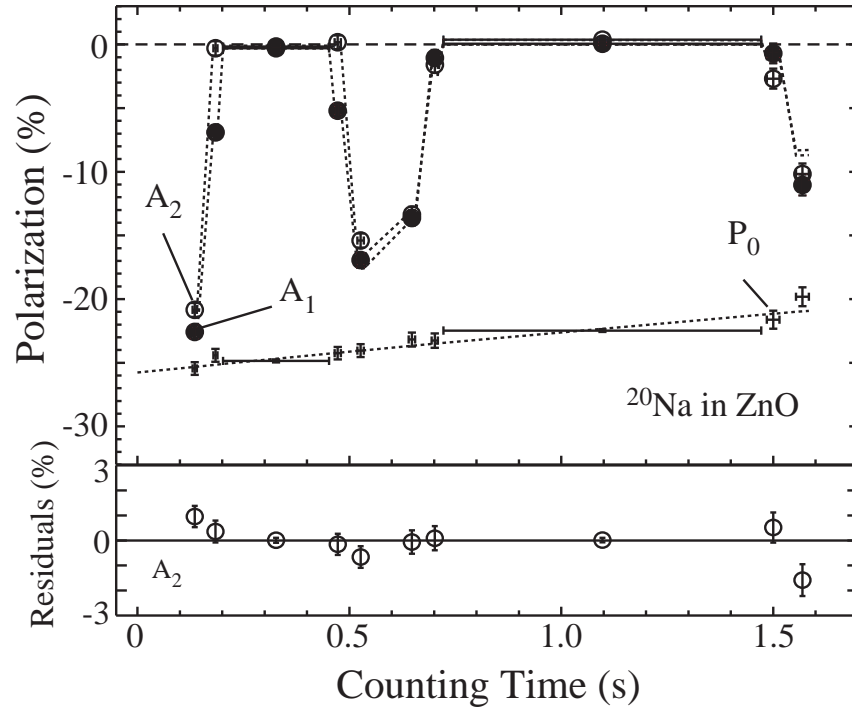


FIG. 12: Results of the spin manipulation for  $^{20}\text{Na}$  in Mg. See the figure caption for Fig. 10. for details.

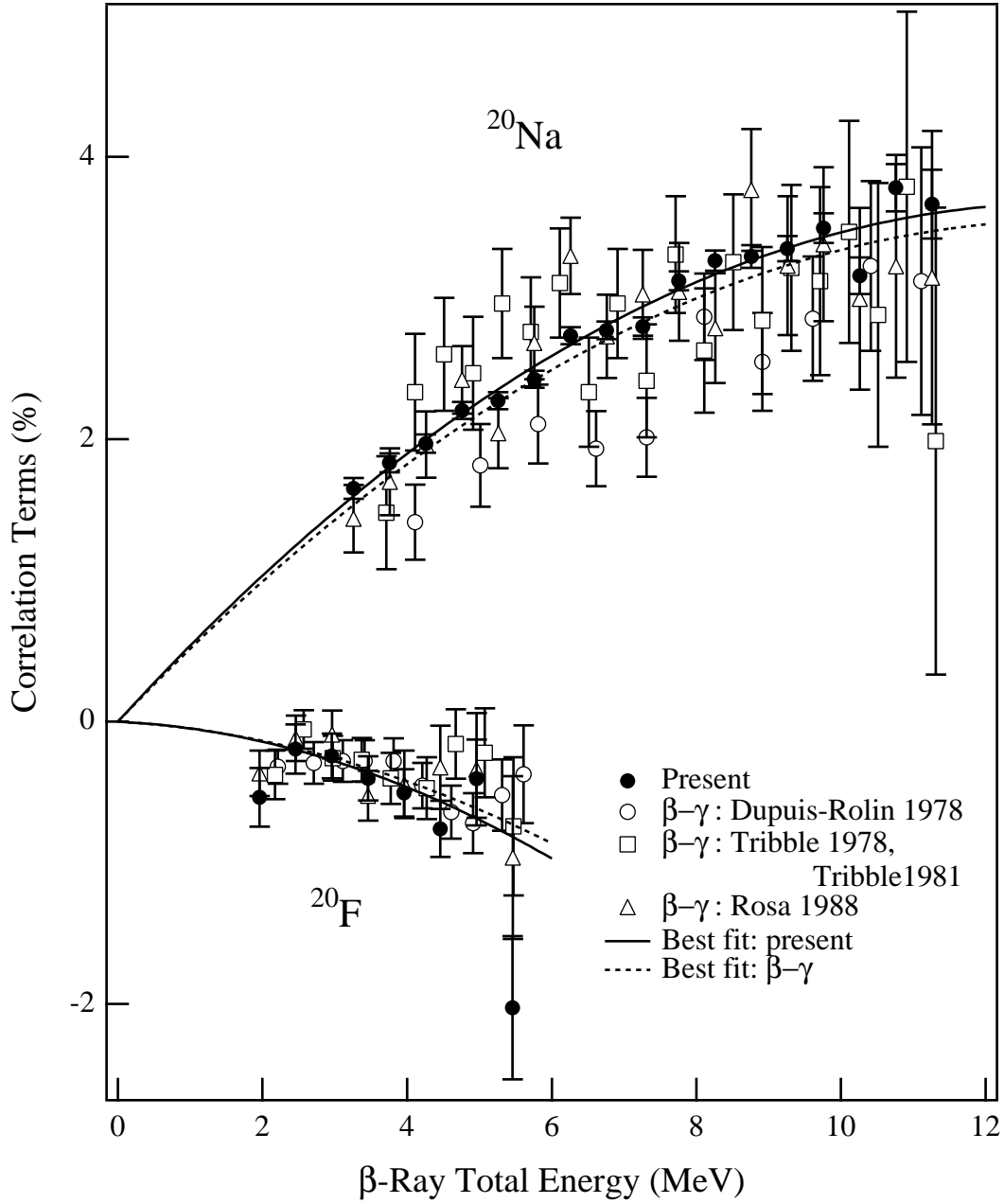


FIG. 13: Result of the alignment correlation terms and  $\beta$ - $\gamma$  correlation terms. The solid circles are the present data, the open circles, squares and triangles are the  $\beta$ - $\gamma$  correlation terms for Dupuis-Rolin 1978: [14], Tribble 1978: [15], Tribble 1981: [16] and Rosa 1988: [17], respectively. The solid curves are the best fit of Eq. (4) to the alignment correlation terms and the dashed curves are for the normalized  $\beta$ - $\gamma$  correlation terms discussed in the text.

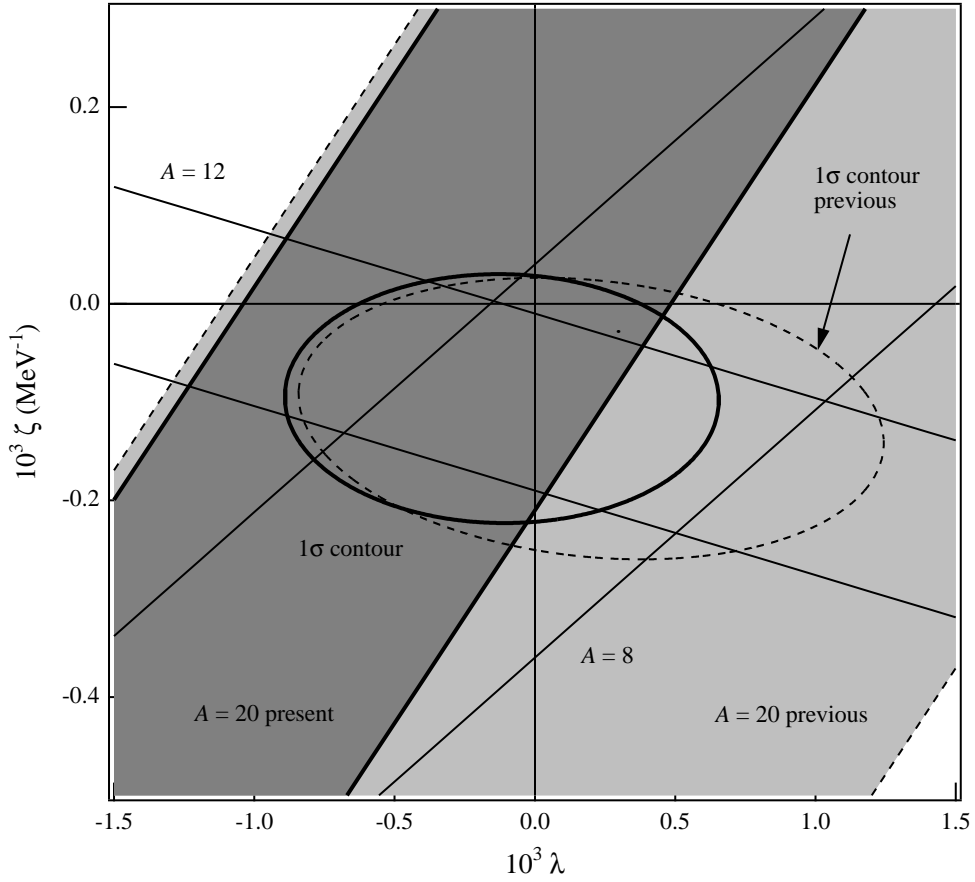


FIG. 14: KDR parameter space with  $L$  calculated without short range correlation. The shaded area is the present result and the light-shaded area is the previous result for the  $A = 20$  system. The solid ellipsoid corresponds to a  $1\sigma$  contour determined by the present result and other  $\beta$ -decay correlation term measurements in the  $A = 8$  [18] and 12 [9] systems, which are indicated by parallel lines. The dashed ellipsoid is a  $1\sigma$  contour with the previous result for the  $A = 20$  system.

TABLE I: Experimental conditions for the spin manipulation.

	$^{20}\text{F}$	$^{20}\text{Na}$	
Single Crystal	$\text{MgF}_2$	Mg	ZnO
Thickness ( $\mu\text{m}$ )	$100 \pm 10$	$200 \pm 50$	$100 \pm 10$
Structure	rutile	hcp	hcp (wurtzite)
$ eqQ/h (\text{kHz})$	$5770 \pm 20$ [25]	$36.7 \pm 0.5^a$	$690 \pm 12^a$ [27]
$\eta$	$0.317 \pm 2$ [25]	0	0
$c$ -axis	$c \parallel H_0$	$c \parallel H_0$	$c \perp H_0$
$Z$ -axis	$Z \perp H_0 (X \parallel H_0)$	$Z \parallel H_0$	$Z \perp H_0$
$\lambda_{\mathcal{P}} (\text{s}^{-1})$	$0.015 \pm 0.003$	$0.26 \pm 0.02$	$0.12 \pm 0.02$
Magnetic Field $H_0(\text{Oe})$	2500	$5286 \pm 5$	
$\mu/\mu_{\text{N}}$	$+2.0935 \pm 0.0009$	$+0.3694 \pm 0.0002$	
Transition ( $m \leftrightarrow m - 1$ )	Frequency $\pm$ FM (kHz)		
$+2 \leftrightarrow +1$	$1223 \pm 125$	$731.5 \pm 4$	$860 \pm 30$
$+1 \leftrightarrow 0$	$2189 \pm 100$	$740.5 \pm 4$	$800 \pm 30$
$0 \leftrightarrow -1$	$2461 \pm 100$	$750.5 \pm 4$	$720 \pm 30$
$-1 \leftrightarrow -2$	$2591 \pm 100$	$759.5 \pm 4$	$610 \pm 30$

<sup>a</sup>Signs are not known but  $eqQ/h$  of  $^{20}\text{Na}$  in Mg and ZnO have opposite signs based on the signs of alignments produced in the spin manipulation.

TABLE II: Experimental conditions for rf in NMR.

RF coil	$^{20}\text{F}$	$^{20}\text{Na}$
Number of turns	$10 \times 10$ turns	$40 \times 40$ turns
Inductance	$6.5 \mu\text{H}$	$54 \mu\text{H}$
DC character of $H_1$	$3.3 \text{ Oe/A}$	$8.3 \text{ Oe/A}$
AFP	$^{20}\text{F}$	$^{20}\text{Na}$
$H_1$ (Typical)	10 Oe	7 Oe
RF time	3 ms	10 ms
Depolarization	$^{20}\text{F}$	$^{20}\text{Na}$
$H_1$ (Typical)	7 Oe	4 Oe
RF time	50 ms	50 ms
Number of sweeps (Typical)	17.5	6.5

TABLE III: Results of the fit to the spin manipulation data. The degree of alignment and effective orientations in counting sections III and VIII were calculated using those parameters. The  $\mathcal{T}$  and  $\mathcal{Q}$  are orientations of rank 3 and 4, respectively, where  $\delta\mathcal{T} \equiv (\mathcal{T}_1^{\text{III}} - \mathcal{T}_1^{\text{VIII}}) + (\mathcal{T}_2^{\text{VIII}} - \mathcal{T}_2^{\text{III}})$  and  $\tilde{\mathcal{Q}} \equiv (\mathcal{Q}_1^{\text{III}} - \mathcal{Q}_1^{\text{VIII}}) + (\mathcal{Q}_2^{\text{VIII}} - \mathcal{Q}_2^{\text{III}})$ .

	$^{20}\text{F}$		$^{20}\text{Na}$	
catcher	MgF <sub>2</sub>	Mg	ZnO	
Initial orientation				
$a_2$	0.241(3)	0.099(4)	0.114(4)	
$a_1$	0.217(3)	0.118(4)	0.127(2)	
$a_0$	0.195(3)	0.164(6)	0.149(6)	
$a_{-1}$	0.186(4)	0.225(7)	0.230(6)	
$a_{-2}$	0.163(3)	0.401(6)	0.392(5)	
Polarization				
$\lambda_{\mathcal{P}}$ (1/s)	0.0154(30)	0.256(21)	0.120(22)	
$\mathcal{P}_0$ (%)	9.53(27)	-36.53(81)	-25.77(64)	
NMR efficiency				
$\eta$ (%)	97.5(2)	97.3(2)	97.6(1)	
$\delta_1$	0.04(12)	0.02(12)	-0.25(13)	
$\delta_2$	-0.19(36)	-0.73(36)	-0.39(10)	
$\delta_3$	-0.06(30)	-0.63(30)	0.38(32)	
$\delta_4$	-0.29(12)	0.31(12)	0.15(20)	
Degree of alignment				
$\mathcal{A}_1^{\text{III}}$ (%)	7.96(18)	-28.36(34)	-23.91(29)	
$\mathcal{A}_1^{\text{VIII}}$ (%)	-4.04(21)	13.79(92)	13.40(10)	
$\mathcal{A}_2^{\text{III}}$ (%)	-7.52(21)	29.32(31)	22.43(29)	
$\mathcal{A}_2^{\text{VIII}}$ (%)	3.96(19)	-13.22(70)	-14.2(11)	
Effective orientation				
$\delta\mathcal{P}$ (%)	-1.20(16)	1.92(32)	0.11(15)	
$\tilde{\mathcal{A}}$ (%)	23.71(77)	-84.3(18)	-74.1(20)	
$\delta\mathcal{T}$ (%)	-0.65(78)	1.4(12)	-3.9(10)	
$\tilde{\mathcal{Q}}$ (%)	-3.12(92)	12.42(84)	10.2(14)	

TABLE IV: Summary of corrections for  $^{20}\text{F}$  in  $\text{MgF}_2$ .  $C$  is the total correction of individual corrections  $C_i$ , except  $D_\gamma$ , which is subtracted from the alignment term.  $\Delta$  indicates uncertainty of the correction.

$E_k$ (MeV)	$C_{\text{res}}$	$\frac{\Delta C_{\text{res}}}{C_{\text{res}}}$	$C_\Omega$	$\frac{\Delta C_\Omega}{C_\Omega}$	$C_{p/E}$	$\frac{\Delta C_{p/E}}{C_{p/E}}$	$C_{B_1}$	$\frac{\Delta C_{B_1}}{C_{B_1}}$	$\frac{\Delta C_{\text{mix}}}{C_{\text{mix}}}$	$\frac{\Delta \bar{A}}{\bar{A}}$	$C$	$\frac{\Delta C}{C}$	$D_\gamma \times 10^2$	$\frac{\Delta D_\gamma}{D_\gamma}$
0.95	0.796	0.043	1.685	0.052	1.099	0.011	0.998	0.031	0.046	0.045	1.471	0.099	0.070	0.086
1.45	0.896	0.019	1.402	0.032	1.057	0.004	0.998	0.031	0.035	0.045	1.325	0.075	0.180	0.100
1.95	0.939	0.011	1.255	0.022	1.034	0.001	0.998	0.031	0.025	0.045	1.216	0.065	0.185	0.108
2.45	0.962	0.006	1.177	0.016	1.021	0.001	0.998	0.031	0.015	0.044	1.154	0.059	0.020	0.650
2.95	0.978	0.004	1.130	0.012	1.013	0.000	0.998	0.031	0.006	0.044	1.117	0.056	-0.143	0.112
3.45	0.992	0.003	1.101	0.010	1.008	0.000	0.998	0.031	0.001	0.044	1.099	0.055	-0.350	0.086
3.95	1.008	0.004	1.082	0.008	1.004	0.000	0.998	0.031	0.000	0.044	1.093	0.055	-0.699	0.086
4.45	1.032	0.006	1.069	0.007	1.002	0.000	0.998	0.031	0.000	0.043	1.103	0.054	-1.472	0.086
4.95	1.090	0.011	1.061	0.008	1.001	0.000	0.998	0.031	0.000	0.043	1.155	0.055	-4.058	0.092
5.45	1.291	0.039	1.062	0.008	1.001	0.000	0.998	0.031	0.000	0.043	1.370	0.066	-16.354	0.136

TABLE V: Summary of corrections for  $^{20}\text{Na}$  in ZnO.  $C$  is the total correction of individual corrections  $C_i$ , except  $D_\gamma$ , which is subtracted from the alignment term.  $\Delta$  indicates uncertainty of the correction.

$E_k(\text{MeV})$	$C_{\text{res}}$	$\frac{\Delta C_{\text{res}}}{C_{\text{res}}}$	$C_\Omega$	$\frac{\Delta C_\Omega}{C_\Omega}$	$C_{p/E}$	$\frac{\Delta C_{p/E}}{C_{p/E}}$	$C_{B_1}$	$\frac{\Delta C_{B_1}}{C_{B_1}}$	$C_{\text{br}}$	$\frac{\Delta C_{\text{br}}}{C_{\text{br}}}$	$\frac{\Delta \bar{A}}{\bar{A}}$	$C$	$\frac{\Delta C}{C}$	$D_\gamma \times 10^2$	$\frac{\Delta D_\gamma}{D_\gamma}$
1.75	0.784	0.093	1.867	0.153	1.04	0.009	1.042	0.025	1.437	0.046	0.031	2.279	0.189	0.071	0.197
2.25	0.878	0.048	1.592	0.091	1.029	0.003	1.042	0.025	1.302	0.042	0.031	1.951	0.118	0.162	0.086
2.75	0.928	0.025	1.427	0.063	1.021	0.001	1.042	0.025	1.216	0.037	0.031	1.713	0.087	0.134	0.09
3.25	0.956	0.015	1.318	0.048	1.015	0.001	1.042	0.025	1.162	0.031	0.031	1.549	0.071	0.121	0.099
3.75	0.974	0.009	1.243	0.037	1.011	0	1.042	0.025	1.114	0.023	0.031	1.421	0.06	0.097	0.134
4.25	0.985	0.005	1.19	0.029	1.008	0	1.042	0.025	1.069	0.016	0.031	1.316	0.052	0.057	0.175
4.75	0.992	0.003	1.151	0.025	1.006	0	1.042	0.025	1.031	0.008	0.031	1.234	0.048	0.043	0.279
5.25	0.998	0.002	1.123	0.021	1.005	0	1.042	0.025	1.007	0.003	0.031	1.182	0.045	0.028	0.5
5.75	1.001	0.001	1.101	0.017	1.004	0	1.042	0.025	1	0	0.031	1.153	0.043	-0.018	0.667
6.25	1.004	0.001	1.084	0.016	1.003	0	1.042	0.025	1	0	0.031	1.137	0.043	-0.052	0.25
6.75	1.006	0.001	1.071	0.014	1.002	0	1.042	0.025	1	0	0.031	1.125	0.042	-0.104	0.154
7.25	1.008	0.001	1.06	0.012	1.001	0	1.042	0.025	1	0	0.031	1.114	0.042	-0.179	0.078
7.75	1.009	0.001	1.051	0.01	1.001	0	1.042	0.025	1	0	0.031	1.106	0.041	-0.226	0.066
8.25	1.011	0.001	1.044	0.01	1	0	1.042	0.025	1	0	0.031	1.1	0.041	-0.293	0.065
8.75	1.012	0.002	1.038	0.009	1	0	1.042	0.025	1	0	0.031	1.095	0.041	-0.384	0.063
9.25	1.013	0.002	1.033	0.009	1	0	1.042	0.025	1	0	0.031	1.09	0.041	-0.539	0.059
9.75	1.014	0.003	1.028	0.008	0.999	0	1.042	0.025	1	0	0.031	1.085	0.041	-0.772	0.062
10.25	1.016	0.004	1.025	0.007	0.999	0	1.042	0.025	1	0	0.031	1.084	0.041	-1.179	0.064
10.75	1.019	0.006	1.022	0.007	0.999	0	1.042	0.025	1	0	0.031	1.084	0.041	-2.112	0.087
11.25	1.024	0.01	1.02	0.007	0.999	0	1.042	0.025	1	0	0.031	1.087	0.042	-4.221	0.138
11.75	1.03	0.015	1.019	0.006	0.999	0	1.042	0.025	1	0	0.031	1.093	0.043	-7.433	0.147
12.25	1.036	0.021	1.018	0.006	0.999	0	1.042	0.025	1	0	0.031	1.098	0.045	-5.826	0.082

TABLE VI: Summary of corrections for  $^{20}\text{Na}$  in Mg.  $C$  is the total correction of individual corrections  $C_i$ , except  $D_\gamma$ , which is subtracted from the alignment term.  $\Delta$  indicates uncertainty of the correction.

$E_k(\text{MeV})$	$C_{\text{res}}$	$\frac{\Delta C_{\text{res}}}{C_{\text{res}}}$	$C_\Omega$	$\frac{\Delta C_\Omega}{C_\Omega}$	$C_{p/E}$	$\frac{\Delta C_{p/E}}{C_{p/E}}$	$C_{B_1}$	$\frac{\Delta C_{B_1}}{C_{B_1}}$	$C_{\text{br}}$	$\frac{\Delta C_{\text{br}}}{C_{\text{br}}}$	$\frac{\Delta \bar{A}}{\bar{A}}$	$C$	$\frac{\Delta C}{C}$	$D_\gamma \times 10^2$	$\frac{\Delta D_\gamma}{D_\gamma}$
1.75	0.831	0.09	1.345	0.096	1.044	0.006	1.042	0.025	1.437	0.046	0.022	1.747	0.144	0.07	0.143
2.25	0.903	0.045	1.231	0.059	1.03	0.002	1.042	0.025	1.302	0.042	0.022	1.553	0.092	0.129	0.078
2.75	0.942	0.024	1.168	0.042	1.021	0.001	1.042	0.025	1.216	0.037	0.022	1.423	0.07	0.106	0.085
3.25	0.966	0.014	1.13	0.033	1.016	0	1.042	0.025	1.162	0.031	0.022	1.343	0.058	0.083	0.084
3.75	0.98	0.009	1.104	0.025	1.011	0	1.042	0.025	1.114	0.023	0.022	1.27	0.049	0.07	0.114
4.25	0.989	0.005	1.086	0.021	1.009	0	1.042	0.025	1.069	0.016	0.022	1.207	0.043	0.047	0.128
4.75	0.995	0.003	1.073	0.018	1.006	0	1.042	0.025	1.031	0.008	0.022	1.154	0.039	0.02	0.35
5.25	1	0.002	1.063	0.015	1.005	0	1.042	0.025	1.007	0.003	0.022	1.121	0.037	-0.016	0.188
5.75	1.003	0.001	1.056	0.013	1.004	0	1.042	0.025	1	0	0.022	1.108	0.036	-0.045	0.156
6.25	1.005	0.001	1.049	0.011	1.003	0	1.042	0.025	1	0	0.022	1.102	0.035	-0.088	0.091
6.75	1.007	0.001	1.045	0.011	1.002	0	1.042	0.025	1	0	0.022	1.099	0.035	-0.141	0.064
7.25	1.009	0.001	1.041	0.01	1.001	0	1.042	0.025	1	0	0.022	1.096	0.035	-0.191	0.063
7.75	1.01	0.001	1.037	0.009	1.001	0	1.042	0.025	1	0	0.022	1.092	0.034	-0.255	0.063
8.25	1.011	0.002	1.035	0.008	1	0	1.042	0.025	1	0	0.022	1.09	0.034	-0.309	0.061
8.75	1.012	0.002	1.033	0.008	1	0	1.042	0.025	1	0	0.022	1.089	0.034	-0.393	0.064
9.25	1.013	0.003	1.031	0.007	1	0	1.042	0.025	1	0	0.022	1.088	0.034	-0.528	0.063
9.75	1.015	0.004	1.029	0.007	0.999	0	1.042	0.025	1	0	0.022	1.087	0.034	-0.766	0.061
10.25	1.017	0.005	1.027	0.007	0.999	0	1.042	0.025	1	0	0.022	1.087	0.034	-1.199	0.065
10.75	1.02	0.007	1.026	0.006	0.999	0	1.042	0.025	1	0	0.022	1.089	0.034	-2.102	0.086
11.25	1.024	0.01	1.025	0.006	0.999	0	1.042	0.025	1	0	0.022	1.093	0.035	-4.074	0.136
11.75	1.03	0.015	1.025	0.007	0.999	0	1.042	0.025	1	0	0.022	1.099	0.037	-6.837	0.142
12.25	1.036	0.021	1.026	0.007	0.999	0	1.042	0.025	1	0	0.021	1.106	0.04	-5.174	0.085

TABLE VII: Correction for contamination in the  $^{20}\text{F}$  spectrum, used in the extraction of polarization.

counting section	I	II	III	VI	V
$C_{\text{mix}}$	$0.975 \pm 0.001$	$0.976 \pm 0.001$	$0.977 \pm 0.001$	$0.979 \pm 0.001$	$0.980 \pm 0.001$

counting section	VI	VII	VIII	IX	X
$C_{\text{mix}}$	$0.981 \pm 0.001$	$0.981 \pm 0.001$	$0.984 \pm 0.001$	$0.986 \pm 0.001$	$0.987 \pm 0.001$

TABLE VIII: Correction for contamination in the  $^{20}\text{F}$  spectrum.

$E_k$ (MeV)	$C_{\text{mix}}(\text{III}, E_k)$	error	$C_{\text{mix}}(\text{VIII}, E_k)$	error
0.95	0.6835	0.0063	0.7131	0.0054
1.45	0.7279	0.0062	0.7794	0.0052
1.95	0.7843	0.0055	0.8355	0.0044
2.45	0.8572	0.0040	0.8937	0.0031
2.95	0.9391	0.0019	0.9557	0.0014
3.45	0.9898	0.0003	0.9927	0.0002
3.95	0.9996	0	0.9997	0
4.45	1	0	1	0
4.95	1	0	1	0
5.45	1	0	1	0

TABLE IX: Corrected alignment correlation terms of  $^{20}\text{F}$  measured in  $\text{MgF}_2$ . The total energy,  $E_{\text{tot}}$  is defined as  $E_{\text{tot}} = E_k + m_e$ , with  $E_k$  and  $m_e$  being the kinetic energy of the  $\beta$  particle and the electron mass, respectively. The first and second errors are the statistical and systematic error, respectively.

$E_{\text{tot}}$ (MeV)	$\left[\frac{B_2}{B_0}\right] \times 10^2$
1.46	$-0.11 \pm 0.28 \pm 0.01$
1.96	$-0.54 \pm 0.21 \pm 0.04$
2.46	$-0.19 \pm 0.17 \pm 0.03$
2.96	$-0.24 \pm 0.16 \pm 0.02$
3.46	$-0.40 \pm 0.16 \pm 0.03$
3.96	$-0.50 \pm 0.17 \pm 0.04$
4.46	$-0.76 \pm 0.20 \pm 0.08$
4.96	$-0.40 \pm 0.28 \pm 0.14$
5.46	$-2.03 \pm 0.51 \pm 0.44$
5.96	$0.50 \pm 1.50 \pm 3.10$

TABLE X: Corrected alignment correlation terms for  $^{20}\text{Na}$ . Results obtained in Mg and ZnO crystals are summarized. Corrections were made separately for the data obtained in Mg and ZnO. The weighted mean was taken as the final result. The first and second errors are the statistical and systematic error, respectively.

$E_{\text{tot}}$ (MeV)	$\left[\frac{B_2}{B_0}\right] \times 10^2$		
	in Mg	in ZnO	weighted mean
2.26	$1.09 \pm 0.12$	$0.68 \pm 0.17$	$0.95 \pm 0.10 \pm 0.14$
2.76	$1.41 \pm 0.10$	$1.70 \pm 0.14$	$1.51 \pm 0.08 \pm 0.17$
3.26	$1.59 \pm 0.09$	$1.76 \pm 0.12$	$1.65 \pm 0.07 \pm 0.13$
3.76	$1.86 \pm 0.09$	$1.79 \pm 0.11$	$1.83 \pm 0.07 \pm 0.12$
4.26	$1.84 \pm 0.08$	$2.15 \pm 0.10$	$1.97 \pm 0.06 \pm 0.11$
4.76	$2.12 \pm 0.08$	$2.32 \pm 0.09$	$2.21 \pm 0.06 \pm 0.11$
5.26	$2.25 \pm 0.08$	$2.30 \pm 0.09$	$2.27 \pm 0.06 \pm 0.10$
5.76	$2.44 \pm 0.08$	$2.41 \pm 0.09$	$2.43 \pm 0.06 \pm 0.10$
6.26	$2.75 \pm 0.08$	$2.71 \pm 0.09$	$2.73 \pm 0.06 \pm 0.11$
6.76	$2.73 \pm 0.08$	$2.82 \pm 0.09$	$2.77 \pm 0.06 \pm 0.11$
7.26	$2.62 \pm 0.09$	$3.02 \pm 0.10$	$2.80 \pm 0.06 \pm 0.11$
7.76	$3.07 \pm 0.09$	$3.18 \pm 0.10$	$3.12 \pm 0.07 \pm 0.12$
8.26	$3.26 \pm 0.10$	$3.26 \pm 0.11$	$3.26 \pm 0.07 \pm 0.12$
8.76	$3.17 \pm 0.11$	$3.43 \pm 0.12$	$3.29 \pm 0.08 \pm 0.13$
9.26	$3.25 \pm 0.12$	$3.46 \pm 0.13$	$3.35 \pm 0.09 \pm 0.13$
9.76	$3.37 \pm 0.15$	$3.63 \pm 0.15$	$3.49 \pm 0.11 \pm 0.14$
10.26	$2.86 \pm 0.18$	$3.44 \pm 0.18$	$3.16 \pm 0.13 \pm 0.13$
10.76	$3.81 \pm 0.25$	$3.75 \pm 0.23$	$3.78 \pm 0.17 \pm 0.16$
11.26	$3.62 \pm 0.38$	$3.70 \pm 0.32$	$3.67 \pm 0.24 \pm 0.24$
11.76	$3.44 \pm 0.67$	$3.35 \pm 0.51$	$3.38 \pm 0.41 \pm 0.63$
12.26	$0.40 \pm 1.32$	$2.50 \pm 0.96$	$1.78 \pm 0.78 \pm 1.13$
12.76	$2.21 \pm 1.94$	$0.90 \pm 1.81$	$1.51 \pm 1.32 \pm 0.51$

TABLE XI: Form factors obtained in the present study. These matrices were extracted from simultaneous fits of the theoretical curve to the present and  $\beta$ - $\gamma$  data. The weak magnetism term  $b/Ac = 8.58 \pm 0.28$  was used for extraction of  $d_{\text{II}}/Ac$ . An average of analyses 2 and 3 was taken as the final result. For the extraction of  $j_2$ ,  $g/A^2c = -53_{-24}^{+46}$  [30] was used.

Analysis Matrix	1: present and [14]				2: present and [15, 16]				3: present and [17]				average of 2 and 3			
	stat.	syst.	total		stat.	syst.	total		stat.	syst.	total		stat.	syst.	total	
$(b - d_{\text{II}})/Ac$	7.33	0.23	0.27	0.35	8.41	0.31	0.22	0.38	8.40	0.30	0.24	0.38	8.41	0.31	0.24	0.39
$d_{\text{I}}/Ac$	5.71	0.53	0.30	0.61	8.49	0.70	0.29	0.76	7.50	0.57	0.35	0.67	8.00	0.64	0.35	0.73
$j_2/A^2c$	149	118	108	160	27	91	100	135	-69	75	82	111	-21	83	100	130
$j_3/A^2c$	-741	162	103	192	-1402	214	76	227	-1144	175	82	193	-1273	195	82	211
$d_{\text{II}}/Ac$	1.25	0.36	0.27	0.45	0.17	0.42	0.22	0.47	0.18	0.41	0.24	0.48	0.18	0.42	0.24	0.48

TABLE XII: Systematic errors for  $d_{\parallel}/Ac$ .

Contribution	Analysis	
	2: present and [15, 16]	3: present and [17]
response of the energy detection system	0.02	0.02
solid angle	0.12	0.13
longitudinal polarization of electron	0.00	0.00
polarization correlation term	0.09	0.10
$\beta$ -decay branches of $^{20}\text{Na}$	0.04	0.06
contaminants in $^{20}\text{F}$ energy spectra	0.00	0.00
alignment calculation	0.10	0.12
anisotropic angular distribution of 1.634 MeV delayed $\gamma$ ray	0.12	0.10
total	0.22	0.24

- 
- [1] S. L. Glashow, Nucl. Phys. **22**, 579 (1961).
- [2] S. Weinberg, Phys. Rev. **112**, 1375 (1958).
- [3] N. Severijns, M. Beck, and O. Naviliat-Cuncic, Rev. Mod. Phys. **78**, 991 (2006).
- [4] P. Herczeg, Prog. Part. Nucl. Phys. **46**, 413 (2001).
- [5] D. H. Wilkinson, Eur. Phys. J. A **7**, 307 (2000).
- [6] L. Grenacs, Ann. Rev. Nucl. Part. Sci. **35**, 488 (1985).
- [7] B. R. Holstein, Rev. Mod. Phys. **46**, 789 (1974).
- [8] J. C. Hardy and I. S. Towner, Phys. Rev. C **79**, 055502 (2009).
- [9] K. Minamisono, K. Matsuta, T. Minamisono, Y. Yamaguchi, T. Sumikama, T. Nagatomo, M. Ogura, T. Iwakoshi, M. Fukuda, M. Mihara, et al., Phys. Rev. C **65**, 015501 (2001).
- [10] K. Kubodera, J. Delorme, and M. Rho, Nucl. Phys. B **66**, 253 (1973).
- [11] R. E. Tribble and G. T. Garvey, Phys. Rev. C **12**, 967 (1975).
- [12] R. D. McKeown, G. T. Garvey, and C. A. Gagliardi, Phys. Rev. C **22**, 738 (1980).
- [13] N. Rolin, J. P. Deutsch, D. Favart, M. Lebrun, and R. Prieels, Phys. Lett. B **70**, 23 (1977).
- [14] N. Dupuis-Rolin, J. P. Deutsch, D. Favart, and R. Prieels, Phys. Lett. B **79**, 359 (1978).
- [15] R. E. Tribble and D. P. May, Phys. Rev. C **18**, 2704 (1978).
- [16] R. E. Tribble, D. P. May, and D. M. Tanner, Phys. Rev. C **23**, 2245 (1981).
- [17] R. D. Rosa, W. W. Daehnick, S. K. Saha, and P. C. Li, Phys. Rev. C **37**, 2722 (1988).
- [18] T. Sumikama, K. Matsuta, T. Nagatomo, M. Ogura, T. Iwakoshi, Y. Nakashima, H. Fujiwara, M. Fukuda, M. Mihara, K. Minamisono, et al., Phys. Lett. B **664**, 235 (2008).
- [19] G. G. Ohlsen et al., Phys. Rev. Lett. **27**, 599 (1971).
- [20] C. D. P. Levy et al., Nucl. Phys. A **701**, 253c (2002).
- [21] E. Arnold et al., Phys. Lett. B **197**, 311 (1987).
- [22] C. D. P. Levy et al., Nucl. Instrum. Methods Phys. Res. B **204**, 689 (2003).
- [23] K. Minamisono, K. Matsuta, T. Minamisono, C. D. P. Levy, T. Nagatomo, M. Ogura, T. Sumikama, J. A. Behr, K. P. Jackson, M. Mihara, et al., Nucl. Instrum. Methods Phys. Res. A **610**, 45 (2010).
- [24] A. Abragam, *The Principles of Nuclear Magnetism* (Oxford University Press, Oxford, 1986).
- [25] H.-J. Stoückman, H. Ackermann, D. Dubbers, M. Grupp, and P. Heitjans, Z. Physik **269**, 47

- (1974).
- [26] K. Minamisono, R. R. Weerasiri, H. L. Crawford, P. F. Mantica, K. Matsuta, T. Minamisono, J. S. Pinter, and J. B. Stoker, Nucl. Instrum. Method Phys. Res. A **589**, 185 (2008).
  - [27] K. Minamisono, K. Matsuta, T. Minamisono, C. Levy, T. Nagatomo, M. Ogura, T. Sumikama, J. Behr, K. Jackson, M. Mihara, et al., Phys. Lett. B **672**, 120 (2009).
  - [28] H. Hirayama and Y. Namino, KEK Internal **99-5**, 1 (1999).
  - [29] B. H. Wildenthal, F. P. Calaprice, and W. Chung, Phys. Rev. C **15**, 2178 (1977).
  - [30] L. K. Fifield, F. P. Calaprice, C. H. Zimmerman, M. J. Hurst, A. Pakkanen, T. J. M. Symons, F. Watt, and K. W. Allen, Nucl. Phys. A **288**, 57 (1977).
  - [31] M. Morita and R. S. Morita, Phys. Rev. **110**, 461 (1958).
  - [32] M. Morita, *Beta Decay and Muon Capture* (W. A. Benjamin, Inc., 1973).
  - [33] J. D. Pearson and R. H. Spear, Nucl. Phys. **54**, 434 (1963).
  - [34] S. Mitsunobu and Y. Torizuka, Phys. Rev. Lett. **28**, 920 (1972).
  - [35] T. K. Alexander, B. Y. Underwood, N. Anyas-Weiss, N. A. Jelley, J. Szücs, S. P. Dolan, M. R. Wormald, and K. W. Allen, Nucl. Phys. A **197**, 1 (1972).
  - [36] P. Ingalls, Nucl. Phys. A **265**, 93 (1976).
  - [37] D. E. Alburger and F. P. Calaprice, Phys. Rev. C **12**, 1690 (1975).
  - [38] H. Genz, A. Richter, B. M. Schmitz, and H. Behrens, Nucl. Phys. A **267**, 13 (1976).
  - [39] T. F. Wang, R. N. Boyd, G. J. Mathews, M. L. Roberts, K. E. Sale, M. M. Farrell, M. S. Islam, and G. W. Kolnicki, Nucl. Phys. A **536**, 159 (1992).
  - [40] D. F. Torgerson, K. Wien, and R. D. Macfarlane, Phys. Lett. B **40**, 203 (1972).
  - [41] E. T. H. Clifford, E. Hagberg, J. C. Hardy, H. Schmeing, R. E. Zauma, H. C. Evans, V. T. Koslowsky, U. J. Schrewe, K. S. Sharma, and I. S. Towner, Nucl. Phys. A **493**, 293 (1989).
  - [42] H. Shiomi, Nucl. Phys. A **603**, 281 (1996).
  - [43] K. Kubodera, J. Delorme, and M. Rho, Phys. Rev. Lett. **38**, 321 (1977).
  - [44] M. Oka and K. Kubodera, Phys. Lett. B **90**, 45 (1980).